Platelets sequester extracellular DNA, capturing tumor-derived and free fetal DNA

Authors: Lauren Murphy[1], Jeanne Inchauspé[1,2], Giampiero Valenzano[3], Pamela Holland[4], Nikolaos Sousos[1,5], Hayley L Belnoue-Davis[6], Rong Li[1], Natalie J. Jooss[1], Camelia Benlabiod[1], Eleanor Murphy[1], Zohar Etzioni[2], Emelie Shepherd[2], Lucy Denly[2], Sujata Biswas[5], Lin Chen[2], Jennifer O'Sullivan[1], Michael P Rimmer[4], Abdullah O. Khan[1], Christina Simoglou Karali[1], Nadia Nasreddin[6], Ian S. Hitchcock[7], Milka Koupenova[8], Skirmantas Kriaucionis[2], Jim R. Hughes[1], Eric O'Neill[3], Manu Vatish[9], Paul Rees[10,11], Simon Leedham[6], Michael Desborough[1,5], Adam J. Mead[1,5], Benjamin Schuster-Böckler*[2], Christopher D. Gregory[4], Bethan Psaila*[1,2,5]

Affiliations:

1. MRC Molecular Haematology Unit, MRC Weatherall Institute of Molecular Medicine, Radcliffe Department of Medicine and National Institute of Health Research (NIHR) Oxford Biomedical Research Centre, University of Oxford, Oxford, U.K. OX3 9DS
2. Ludwig Institute for Cancer Research, Nuffield Department of Medicine, University of Oxford, Oxford, U.K. OX3 7DQ
3. Department of Oncology, University of Oxford, Old Road Campus Research Building, Roosevelt Drive, Oxford, U.K. OX3 7DQ
4. Centre for Inflammation Research, Institute for Regeneration and Repair, University of Edinburgh, Edinburgh BioQuarter, 4-5 Little France Drive, Edinburgh, U.K. EH16 4UU,
5. Oxford University Hospitals NHS Foundation Trust, Oxford, U.K. OX3 9DS
6. Wellcome Centre for Human Genetics, University of Oxford, Oxford, U.K. OX3 7BN
7. York Biomedical Research Institute and Department of Biology, University of York, Heslington, York, U.K. YO10 5DD
8. Division of Cardiovascular Medicine, Department of Medicine, University of Massachusetts Chan Medical School, 368 Plantation Street, Worcester, Massachusetts, U.S.A. MA 01605
9. Nuffield Department of Women's and Reproductive Health, University of Oxford, John Radcliffe Hospital, Oxford, U.K. OX3 9DU
10. Department of Biomedical Engineering, Faculty of Science and Engineering, Swansea University, Swansea, Wales, U.K. SA1 8EN
11. Imaging Platform, Broad Institute of MIT and Harvard, Cambridge, MA, U.S.A

*Correspondence to bethan.psaila@ndcls.ox.ac.uk. For computational enquiries: benjamin.schuster-boeckler@ludwig.ox.ac.uk

Abstract

Platelets are anucleate blood cells vital for hemostasis and immunity. During cell death and aberrant mitosis, nucleated cells release DNA, resulting in 'cell free' DNA in plasma (cfDNA). An excess of cfDNA is deleterious. Given their ability to internalize pathogen-derived nucleic acids, we hypothesized that platelets may also clear endogenous cfDNA. We found that despite lacking a nucleus, platelets contained a repertoire of DNA fragments mapping across the nuclear genome. We detected fetal DNA in maternal platelets and cancer-derived DNA in platelets from patients with pre-malignant and cancerous lesions. As current liquid biopsy approaches utilize platelet-depleted plasma, important genetic information contained within platelets is being missed. This study establishes a physiological role for platelets that has not previously been highlighted, with broad translational relevance.

Main Text

Platelets are fundamental to hemostasis, vascular maintenance and both innate and adaptive immunity. Platelets inherit RNAs from their parent megakaryocytes together with translational and splicing machinery. As part of their role in immunity, platelets sense pathogen-derived nucleic acids and internalize DNA and RNA viruses, triggering inflammatory responses (*1-4*). Intriguingly, in addition to pathogen-derived nucleic acids, RNAs originating from solid tumor cells and from inhaled pine tree pollen have also been detected in human platelets (*5, 6*) indicating that platelets internalize RNA from a range of cellular sources during peripheral circulation. While platelet RNA has emerging utility as a liquid biopsy approach for hematological (*7*) and solid malignancies (*8, 9*), whether platelets contain any form of DNA, and if so, its genomic origin, has not been extensively investigated.

During cell death and aberrant mitosis, nucleated cells release chromosomal DNA, resulting in 'cell free' DNA in plasma (cfDNA). Analysis of cfDNA from blood plasma is currently implemented in a wide range of clinical settings, including cancer care (*10-16*) and prenatal testing (*17*). A major obstacle to clinical utility is the low sensitivity in scenarios where the abundance of target DNA is low. We hypothesized that in addition to internalizing pathogen-derived exogenous DNA, platelets may clear endogenous cfDNA from plasma, including DNA fragments released by healthy cells as well as those bearing oncogenic mutations. As conventional methods isolate cfDNA from platelet-depleted plasma, any DNA fragments that are sequestered within platelets would be missed. We therefore also hypothesized that including DNA captured by platelets may add value in diagnostic pathways.

Results

Platelets contain DNA

To determine whether DNA is present within human platelets, platelets were purified from three sources: whole peripheral blood, isolated plasma and 'plateletpheresis' concentrates – clinical-grade platelet pools isolated from healthy donors for transfusion purposes (Fig. 1A). We examined platelets by fluorescence microscopy after labeling purified platelets with NUCLEAR-ID Red DNA, a highly specific, cell permeable dye that intercalates with double stranded (ds) DNA. A proportion of platelets showed a clear signal for the DNA probe (Fig. 1B). To verify that this represented nuclear DNA, we confirmed the presence of a nuclear genomic region of the *TP53* gene in platelet DNA (pDNA, fig. S1A & S1B). Immunofluorescence staining of a peripheral blood smear also showed a clear signal for the DNA stain Hoechst in platelets, confirming that the DNA was not acquired by platelets during purification from whole blood (fig. S1C).

To quantify the proportion of platelets that contained DNA we used flow cytometry, examining positivity for DRAQ5, a dsDNA-specific dye. Most platelets showed low-level DRAQ5 positivity while around 8% were strongly positive (DRAQ5^{hi}, Fig. 1C & fig. S1D). Prior studies have shown that newly produced or 'younger' platelets can be distinguished from 'older' platelets by their higher content of RNA, and that younger platelets also have higher expression of markers of platelet receptor activation or degranulation (*18-20*). Co-staining for RNA and DNA showed that the majority of DRAQ5^{hi} platelets were low or negative for RNA (Fig. 1D, fig. S1E), indicating that

DNA is present in both newly produced (RNA-high) platelets as well as in older (RNA-low) platelets. Comparing DRAQ5^{hi} vs. DRAQ5^{lo} platelets showed that DRAQ5^{hi} platelets contained more RNA and had higher expression of markers of activation than DRAQ5$^{lo/neg}$ platelets, implying that the DNA content of platelets also decreased during platelet lifespan and after platelet activation, in parallel with RNA content (Fig. 1D & 1E).

To investigate platelet content of DNA in a larger cohort, we extracted pDNA from peripheral blood of 76 adult donors (table S1 – 4). The extremely high purity of the platelet pellets was confirmed by flow cytometry analysis and cytospin preparations (fig. S1A, S1F & S1G). DNA was obtained from both the platelet pellet and platelet-depleted plasma (cfDNA) in all cases, with a higher yield of DNA from platelet pellets than from matched platelet-depleted plasma (i.e. a conventional cfDNA preparation). In this cohort, a median abundance of 7.18 genomic copies was isolated from platelets per µl of blood plasma, which equates to approximately 0.000012 genomic equivalents of DNA per platelet (fig. S1H).

Platelets sequester DNA during circulation

To determine whether the DNA detected in platelets was captured during peripheral circulation or solely derived from parent megakaryocytes (*21*), we collected antenatal blood samples and looked for fragments of the Y-chromosome in platelets of mothers with uncomplicated pregnancies carrying male offspring (table S5). Using Y-chromosome fluorescence *in situ* hybridization, Y-chromosome fragments were visualized in the platelets of mothers carrying a male fetus (Fig. 1F, movie S1). In 100% of samples (n = 30), we correctly ascertained the sex of the fetus by the presence or absence of the Y-chromosome gene *SRY* alleles in maternal platelets (Fig. 1F). *SRY* remained detectable in platelets at 24 and 48 hours after delivery of the baby (fig. S1I) and was not detected in mononuclear cells (Fig. 1F) or red blood cells (fig. S1J) from the same blood samples, indicating that free fetal DNA could be detected exclusively in maternal platelets. This suggested that the detection of *SRY* in maternal platelets was not due to 'contaminating' cfDNA in the cell pellets, nor the presence of fetal blood cells in the maternal circulation. While cross-placental transfer of fetal platelets cannot be fully excluded, this observation confirmed the presence of nuclear DNA within platelets.

Platelets 'clear' cfDNA from plasma

We reasoned that if platelets were clearing cfDNA from plasma, then the abundance of cell/platelet-free DNA in plasma would increase if the platelet count was reduced. To test this, we induced acute and specific antibody-mediated depletion of platelets in mice. In accordance with our hypothesis, induction of immune thrombocytopenia led to an acute rise in plasma cfDNA concentration (Fig. 1G). Similarly, we found higher concentrations of plasma cfDNA in patients with immune thrombocytopenic purpura (ITP) who had severely low platelet counts ($< 20 \times 10^9$/L), as compared to those with normal platelet counts (Fig. 1H, table S6, $^*P < 0.05$, n = 23).

Together, these data indicate a biological role for platelets in the clearance of cfDNA from plasma.

Platelets rapidly capture DNA from nucleated cells

To confirm that platelets sequestered chromosomal fragments released from nucleated cells, we used live cell imaging to visualize DNA uptake *in vitro*. Colorectal adenocarcinoma cells

(COLO205) were labeled with DNA probes and washed twice to remove any non-internalized probe prior to co-incubation with platelets. Rapid acquisition of COLO205 cell-derived DNA by platelets was observed (Fig. 2A & 2B, figs. S2A-C, movies S2 & S3). The average DNA fluorescence intensity of the 168 platelets imaged plateaued at ~6 minutes, suggestive of saturation of DNA uptake (Fig. 2C).

DNA is internalized and released on platelet activation

To determine the localization of platelet DNA, we performed high-resolution Airyscan imaging of healthy donor platelets spread on collagen-coated glass coverslips. During spreading, platelets evaginate the membranes of their open canalicular system (OCS) - an internal surface-connected system of channels - in order to increase their surface area (*22*). This process extrudes materials captured within the OCS and pushes intracellular contents to the center (*22*). Imaging of spread platelets co-stained for P-selectin (CD62P) - a marker of platelet activation and de-granulation - and DRAQ5 revealed that DNA was located at the center of spread platelets (Fig. 2D). Calculation of the DRAQ5 staining intensity during progressive computational erosion of the CD62P mask from the edge of the platelet to the center further confirmed that DNA was internalized within the body of the platelet and not held within the OCS (fig. S2D).

We next performed co-localization analyses by co-staining platelets for DNA (DRAQ5), the different types of platelet storage granules (alpha and dense granules), and other organelle markers. We observed strong co-localization between DNA and membrane-bound internal vesicles (CD81 and LAMP-2), with no correlation with mitochondria (TOM20, Fig. 2E-H), confirming that the DNA content of platelets was largely contained within membrane-bound vesicles, and not stored in granules or restricted to mitochondrial DNA.

Platelets internalize DNA-loaded extracellular vesicles (EVs)

DNA-loaded EVs are released during cellular apoptosis, and viable cells also remove excess cytoplasmic DNA created during aberrant cycles of mitosis by the release of DNA-loaded EVs (*23*-*27*). Platelets internalize EVs through their OCS and endocytosis (*28*), and platelet uptake of tumor cell-derived EVs has previously been shown to transfer cancer cell-derived protein cargo and mRNA transcripts (*29*).

We therefore investigated whether EVs may mediate DNA transfer to platelets. Platelets isolated from female donors were incubated with EVs derived from male lymphoma BL2 cells or isogenic BL2 cells engineered to over express the apoptosis-suppressing gene *BCL2* (BL2-Bcl-2 cells). This system enabled us to also explore whether DNA-loading of EVs occurred during apoptosis. EVs were isolated from BL2 and BL2-Bcl-2 cells after UV irradiation, generating apoptotic EVs (apo-EVs) from BL2 cells or non-apoptotic (non-apo EVs) from BL2-Bcl-2 cells. The EVs were treated with DNase to remove any non-internalized DNA (Fig. 2I). DNA-loaded EVs were visible adherent to, as well as within, platelets following co-incubation (Fig. 2J & 2K, movies S4 & S5, fig. S2E & S2F). Copies of *SRY* were detectable in platelets from female donors only following incubation with BL2-derived EVs, and in higher abundance following co-incubation with apo-EVs than with non-apo EVs (Fig. 2L & fig. S2G). Similarly, using whole chromosome X and Y FISH probes, fragments of both X- and Y-chromosomes were visualized in female platelets following co-incubation with HEL cells that also derive from a male donor (Fig. 2M).

Platelets internalize membrane-free DNA fragments

To test whether platelets could also internalize 'free' DNA fragments that were not contained within EVs, we exposed healthy donor platelets to synthetic DNA fragments ranging from 128 - 657 base pair (bp) lengths. Platelets efficiently internalized all tested DNA fragments, confirming that platelets sequestered non-membrane bound DNA of varying lengths in addition to DNA-loaded EVs (Fig. 2N).

Pharmacological modulation of DNA trafficking

To explore whether DNA uptake and release by platelets could be pharmacologically manipulated, we tested the impact of agonists and inhibitors known to block platelet activation and/or specific components of cargo trafficking. Activation of platelets with the canonical platelet agonist thrombin receptor activating peptide (TRAP) decreased their DNA content (Fig. 3A), indicating that DNA is released by platelets upon activation. In keeping with this, the yield of DNA isolated from platelets was higher when platelets were treated with two potent inhibitors of platelet activation - aspirin and ibrutinib, a BTK inhibitor (Fig. 3B-C & fig. S3A).

We next tested a range of inhibitors known to block specific components of cargo trafficking by platelets, including inhibitors of actin (cytochalasin D), membrane ruffling (imipramine), clathrin (Pitstop 2), caveolae-dependent endocytosis (nystatin), dynamin (Dynole) and Na^+/H^+ exchange/micropinocytosis (amiloride). In keeping with previous literature suggesting that platelets 'engulf' EVs via endocytosis at the OCS membrane, we found that platelet uptake of DNA-loaded apo-EVs was reduced by the dynamin inhibitor Dynole, indicating that DNA-loaded apo-EVs were internalized by clathrin-mediated endocytosis (Fig. 3E-F).

These inhibitors did not reduce the uptake of free DNA fragments by platelets, suggesting that this occurs via an alternative, clathrin-independent mechanism (Fig. 3G). Rather, we found that Dynole and amiloride substantially increased the amount of DNA obtained from the platelets exposed to synthetic DNA fragments (Fig. 3H-I). Dynole and amiloride also block platelet exocytosis and the release of intracellular contents (*30, 31*). Accordingly, we found that Dynole reduced platelet DNA release (Fig. 3J-L).

Together, these data indicated platelet activation was not required for DNA uptake, but that DNA was released by platelets upon activation. Furthermore, platelet content of DNA can be pharmacologically modulated to increase the abundance of DNA preserved within platelets (fig. S3B).

Detecting cancer mutations in platelets

Given the growing importance of cfDNA detection in cancer screening and molecular profiling, we sought to determine whether platelets may take-up tumor-derived DNA fragments that conferred cancer-specific genetic variants.

Platelets from healthy donors were incubated with a variety of human cancer cell lines harboring common cancer-associated gene mutations, including colorectal cells and erythroleukemia cells (Fig. 4A). Analysis of DNA isolated from platelets following co-incubation with cancer cell lines

detected all relevant oncogenic mutations, including *KRAS*G12D, *BRAF*V600E, *PIK3CA*H1047R and *JAK2*V617F (Fig. 4B & 4C). No cancer-specific gene mutations were identified in healthy donor platelets incubated alone, but wild-type alleles were detected (Fig. 4C), indicative of DNA sequestered by platelets prior to blood sampling.

To determine whether the ability to capture extracellular DNA was specific to platelets or shared by other blood cell types, we tested whether *BRAF*V600E derived from COLO205 cells was also sequestered *in vitro* by peripheral blood mononuclear cells (MNCs) and red blood cells (RBCs). While mutant *BRAF (BRAF*V600E) was readily detectable in platelet DNA (pDNA, Fig. 4D), fewer copies of *BRAF*V600E were detected in MNCs and RBCs (Fig. 4D & fig. S3C-E), where they were of negligible abundance in comparison to wild-type alleles (fig. S3D & S3E).

pDNA is protected from nucleases

To test whether pDNA was protected from external nuclease digestion, conditioned media (analogous to cfDNA) and platelets were treated with DNase following conditioning by HEL cells that carry the *JAK2*V617F mutation. Detection of *JAK2*V617F in HEL cell conditioned media was completely abrogated by DNase treatment (Fig. 4E). In contrast, there was no reduction in the abundance of *JAK2*V617F in platelets following DNase treatment (Fig. 4E), indicating that the majority of DNA was encapsulated by the platelet outer membrane and protected from enzymatic degradation. This was verified using synthetic DNA fragments and target-specific primers (fig. S3F).

Genomic distribution and origin of pDNA

We then set out to explore the genomic characteristics of pDNA and validate its utility for detection of cancer gene aberrations *in vivo*.

cfDNA has a classical fragmentation profile with a periodicity reflecting nucleosomal footprints (*12*). Electrophoretic analysis of pDNA showed fragments of around 12’000-16’000 bp, and many samples also showed shorter fragments of around 120-500 bp with nucleosome footprints, similar to the nucleosome footprint of cfDNA (fig. S4A & S4B). Low-input chromatin immunoprecipitation (ChIPmentation) for H3k27 histone acetylation of DNA isolated from platelet pellets and live-cell imaging of platelets co-incubated with H2B-mCherry labeled HEL cells confirmed that the DNA sequestered by platelets was associated with nucleosomes, and that histone modifications are preserved in platelet DNA (fig. S4C & S4D, movie S6).

To compare the genomic origin of pDNA and cfDNA, whole genome sequencing (WGS) was performed on matched pDNA and cfDNA extracted from the peripheral blood of 15 donors, of whom 10 had active malignancy and 5 had undergone surgery and/or chemoradiotherapy, to screen for residual disease (table S4). Size selection was performed on the pDNA to separate the shorter (less than 600 bp) “s-pDNA”, that were similar in length to cfDNA fragments, from the longer fragments ("l-pDNA”).

We performed low pass WGS (mean target coverage of 1x) on s-pDNA, l-pDNA and paired cfDNA (n = 15). Platelets contain a small number of mitochondria, estimated at 4-6 mitochondria per cell (*32, 33*). The majority of fragments from both s- and l-pDNA mapped to the nuclear genome (97.0-

99.9% for s-pDNA and 61.7-99.1% for l-pDNA, Fig. 4F). As expected, given that the mitochondrial genome is ~16'500 bp, a higher subfraction (0.9-30.1%) of l-pDNA mapped to the mitochondrial genome, vs. 0.081-2.968% of the shorter fragments (Fig. 4F).

Mapping across the genome revealed that pDNA fragments covered the entire nuclear genome (fig. S4E), mirroring cfDNA and demonstrating that sampling of pDNA would enable genetic variants across the genome to be detected. Compared to cfDNA, the s-pDNA fragments showed more even coverage, as indicated by a lower Gini index (*34*) (fig. S4F).

Platelet DNA maps to the nuclear genome, and coverage mirrors cfDNA

We then obtained deeper sequencing (mean sequencing depth 15x ± 3 / 12x ± 1 for cfDNA and s-pDNA, respectively) of paired cfDNA and s-pDNA, including 5 from donors after therapy (samples 1-5), and 2 from donors with active, untreated pancreatic and colorectal carcinoma (table S4). No notable differences were detected in sequencing quality (base quality, 3' bias, mapping rate) between s-pDNA and cfDNA, except for a higher estimated PCR duplication rate (cfDNA: 3.2% ± 0.6%, pDNA: 11.3% ± 7.2%), indicating lower complexity of short pDNA libraries, presumably due to the size selection.

Nucleosome-bound cfDNA is more protected from degradation than nucleosome-free DNA. This leads to a characteristic fragment-length distribution of cfDNA, with mono- and di-nucleosome length peaks at approximately 167 bp and 320 bp (*35*). The peak mean fragment length for s-pDNA was 166 bp ± 0.8, with a second, di-nucleosome peak at approximately 328 bp. The di-nucleosome peak was fractionally, but larger in s-pDNA than cfDNA (fig. S5A), likely reflecting the increased protection of pDNA from nuclease digestion, as observed in our *in vitro* experiments (Fig. 4E & fig. S3F).

cfDNA fragments of tumor cell origin are shorter than wild-type fragments (*36, 37*). In accordance with this, we observed that both mono- and di-nucleosome fragment lengths were notably shorter in both pDNA and cfDNA in sample 6, derived from a patient with an inoperable pancreatic tumor and containing readily detectable tumor-derived cfDNA, indicating that fragmentomic analysis may be applied to platelet DNA to detect the presence of cancer (*38*), and that platelets capture DNA fragments that resemble those found in cfDNA *in vivo* (Fig. 4G, table S4).

To confirm the capture of circulating tumor cell-derived DNA (ctDNA) by platelets *in vivo*, we used iChorCNA (*39*) to look for copy number alterations (CNA) and estimate the fraction of tumor-derived DNA. Clonal amplifications and deletions in chromosomes 6 and 7 as well as sub-clonal amplifications in chromosome 2 were detected in both cfDNA and s-pDNA from sample 6 (from the patient with pancreatic cancer), with an estimated tumor fraction of 25% (Fig. 4H). CNAs detected in s-pDNA mirrored those present in cfDNA, and the estimated proportion of tumor-derived DNA was highly correlated between s-pDNA and cfDNA (fig. S5B & S5C). Selecting DNA fragments smaller than 150 bp increased the estimated tumor content of s-pDNA from 25% to 30%, in parallel to the increase seen in cfDNA (fig. S5D). No CNAs were detected in the l-pDNA from sample 6 (fig. S5E), in line with previous reports that ctDNA is enriched in shorter fragments (*37*), nor in either the cfDNA or pDNA from patients after therapy.

Matched tumor and healthy tissue biopsy samples were available for sample 7 from a patient with colorectal carcinoma, enabling us to look deeper for low-level ctDNA by screening for tumor-specific mutations not present in matched healthy tissue. We compared the detection rate of tumor-specific mutations from the relevant donor with detection of random samples of mutations taken from other patients with colorectal carcinoma (*40*). The matched tumor mutations were detected at a higher rate than the random mutations in the cfDNA and s-pDNA and at similar frequency (likelihood rate 8.92e-11 for cfDNA and 2.30e-07 for s-pDNA), with lower-level detection in the l-pDNA (P <0.0004; Fig. 4I), confirming the presence of ctDNA in platelets.

These data indicated that ctDNA was present within platelets in similar abundance to cfDNA, both in patients with high levels of ctDNA and clear CNAs (>20%, sample 6, Fig. 4H) and in those with extremely low levels (<0.5%, sample 7, Fig. 4I), where targeted analysis and matched tumor tissue was required. Overall, ctDNA was identified in both platelets and cfDNA in 20% of the pre-treatment samples either by detecting CNAs or known tumor mutations, in keeping with the sensitivity of WGS for ctDNA detection reported in large clinical cohorts (*41*).

The enrichment for nucleosome-bound DNA in cfDNA has previously been used to gain insight into gene expression patterns and cell-of-origin, with prior reports showing that a depletion of reads occurs over transcriptional start sites (TSS) with periodicity in coverage relative to the TSS (*42*). In addition, DNA methylation studies have shown that the majority (>90%) of cfDNA in both healthy individuals and in those with cancer is of blood cell origin including neutrophils, monocytes, erythroblasts (*43*) and megakaryocytes (*44*). We found very similar depletion in sequencing coverage and periodicity around TSS for genes that are highly expressed in peripheral blood MNCs in both pDNA and cfDNA, suggesting a shared cellular origin of pDNA and cfDNA (Fig. 4J & fig. S5F). Notably, the depletion in coverage for high-expression MNC genes was less marked for the sample that had an estimated ctDNA fraction of 25% than for the other samples (Fig. 4J).

To orthogonally validate the cell-of-origin of pDNA, whole genome methylation analysis was performed using the bisulfite-free sequencing method, TET-assisted pyridine borane sequencing (TAPS) (*45*). The data was then deconvoluted using a published atlas of cell-specific methylation patterns (*46*). This confirmed a similar cellular origin of pDNA and cfDNA, with the majority originating from blood leukocytes and a minor contribution from hepatocytes. Of note, a higher proportion of l-pDNA than s-pDNA mapped to megakaryocyte-specific loci (35.9% vs. 16.8%), suggesting that more l-pDNA may derive from parent megakaryocytes (fig. S5G).

High abundance of mutant alleles in platelets in colorectal and pancreatic carcinoma

To test whether including an analysis of pDNA would add value to plasma cfDNA in the setting of cancer diagnostics, we used a mouse model of colorectal carcinoma in which expression of *KRAS*G12D and *TP53* mutations are induced via the villin promoter, resulting in locally-invasive colorectal adenocarcinoma with a low incidence of metastases, and mice with *KRAS*G12D$^{/+}$, *TP53*$^{fl/fl}$ plus *NOTCH*$^{fl/+}$, with more aggressive and metastatic disease (*47*) (Fig. 5A). pDNA and cfDNA were extracted simultaneously from the same blood sample (Fig. 5A).

Mutant *KRAS*G12D as well as wild-type *KRAS* alleles were readily detectable in both cfDNA and platelets of mice with colorectal carcinoma. In over half of the mice (13/20, 65%), copies of *KRAS*G12D per µl of DNA were in higher abundance in pDNA than in cfDNA, both in mice with locally invasive and metastatic disease (Fig. 5B-5E).

To corroborate these findings in a second model and examine an early stage during tumorigenesis prior to tumor dissemination, we used an orthotopic pancreatic cancer model where pancreatic cancer cells were inserted within a Matrigel plug into the body of the pancreas (*48*). Fourteen days after implantation and prior to local tumor invasion, *KRAS*G12D alleles were readily detected in murine platelets (Fig. 5C & fig. S6A & S6B), and were not reduced in mice receiving low-dose systemic aspirin therapy (fig. S6C).

***BRAF*V600E in platelets of patients with pre-cancer**

Improving the sensitivity for liquid biopsy screening is crucial in the setting of low tumor-burden disease and in patients with pre-malignant lesions, where the abundance of ctDNA is low. Sessile serrated lesions (SSLs) are high-risk, pre-malignant colon polyps driven by mutations in *BRAF* that account for around one quarter of colorectal cancers (*49*). To explore the utility of pDNA for detecting pre-malignant lesions, we collected platelets and cfDNA from patients found to have SSLs at colonoscopy (n = 31) vs. controls (n = 14).

Mutant *BRAF*V600E alleles were detected in either the cfDNA and/or pDNA in 16.1% of the patients with serrated polyps (5/31, Fig. 5F), consistent with previous reports of the frequency of detectable ctDNA in SSL cohorts (*50, 51*). Mirroring our findings in the CRC mouse model, around half (3/5) of the patients with detectable ctDNA had a higher number of *BRAF*V600E copies in pDNA than in cfDNA (Fig. 5F-H, fig. S6D). *BRAF*V600E was detected in none of the pDNA samples from 14 controls (Fig. 5F), demonstrating high specificity of targeted mutational analysis of platelet DNA in this setting and that at least half of the relevant ctDNA is sequestered by blood platelets.

Discussion

Prior studies of platelet nucleic acid content have only focused on RNA (*8, 52-54*), although the presence of DNA in platelets has been noted by other groups (*3, 4, 21, 55*). For example, a study examining the presence of histone proteins in platelets during sepsis showed that 5-35% of platelets were positive for the DNA-specific marker DRAQ5 (*55*), and the presence of megakaryocyte-derived DNA in platelets was recently corroborated by an independent group (*21*). Here we have performed a detailed interrogation of platelet DNA content, demonstrating a biological role for platelets that was previously unappreciated – as scavengers of endogenous extracellular cfDNA, including tumor-derived and free fetal DNA.

We show that platelet uptake of DNA can occur by multiple mechanisms – endocytosis of DNA-loaded EVs from apoptotic cells, and uptake of membrane-free DNA fragments. Previous reports indicated that DNA can bind to the platelet surface (*56, 57*). We found that DNA was also internalized by platelets and held in membrane-bound vesicles, where it was protected from exogenous DNase degradation and subsequently released upon platelet activation. DNA release

could be prevented using pharmacological inhibitors, thereby preserving the DNA within platelets where it is protected from degradation, increasing the yield of DNA obtained from platelet pellets.

Several physiological mechanisms exist to limit the abundance of cfDNA, as excess extrachromosomal DNA in the cytosol and in plasma is pro-inflammatory (*58, 59*). We demonstrated higher and more variable levels of cfDNA in plasma in the setting of severe thrombocytopenia in both a mouse model and in patients. This supports a role for platelets in regulating the cfDNA content of plasma, although we cannot exclude that the higher level of cfDNA observed was due to other consequences of antibody-mediated platelet clearance.

Further work is required to ascertain whether platelets deploy their DNA content at sites of activation. An attractive hypothesis is that platelet clearance may control the non-specific immunostimulatory activity of cfDNA in plasma, and that platelets may release DNA cargo to evoke an immune response in a targeted fashion at sites of platelet activation. Platelets have also been shown to mediate horizontal transfer of RNAs and transcription factors (*60*), either via uptake of whole platelets by phagocytes, endothelial cells and smooth muscle cells or by the release of platelet-derived microvesicles (*59*). Whether platelets can similarly act as a vector for the horizontal transfer of DNA fragments, including potentially extrachromosomal DNA (*59*), and whether platelets modify sequestered DNA prior to release, remains unknown.

Detection and analysis of cfDNA is rapidly being implemented in several clinical settings including cancer screening, molecular profiling, and detection of residual disease as well as in prenatal diagnosis (*61-63*). Currently, a major limitation is the poor sensitivity for low tumor burden disease. Pre-analytical approaches to increase capture of ctDNA would be of interest. Anucleate red blood cells have also been shown to contain DNA fragments, including cancer-cell derived DNA (*64*). In our studies, we did not detect *SRY* in red cell pellets of pregnant women and a substantially lower ratio of mutant-to-wildtype alleles was observed in red cells than platelets in our co-culture experiments, suggesting a superiority of platelets over red cells for liquid biopsy-based screening approaches. Our data suggested that a substantial proportion of ctDNA is contained within platelets, and that this information is currently missed from standard sampling protocols that extract cfDNA from platelet-depleted plasma. This study paves the way for validation in larger clinical cohorts to test whether combining cfDNA with pDNA adds value, as well as future research to further establish a role for platelets in cfDNA homeostasis.

Materials and methods

Ethical approval, banking and processing of samples

All procedures were performed in accordance with the ethical standards of the Declaration of Helsinki. Patient samples were collected by the Oxford Translational Gastroenterology Unit (TGU) and the Oxford Radcliffe Biobank (ORB). All patients provided informed consent, and procedures were approved by Yorkshire & The Humber - Sheffield Research Ethics Committee (REC reference number: 16/YH/0247), ORB research tissue bank ethics (REC reference 19/SC/0173) and Oxford GI Cohort ethics (REC reference 21\YH\0206).

10 to 20 ml of peripheral blood was drawn into EDTA-coated (Fisher Scientific, cat # 367839) or Cell-Free DNA (Streck, cat # 218997) blood collection tubes from patients presenting with colorectal, esophageal or pancreatic cancer. 10 ml of peripheral blood was collected into Streck tubes, from patients with sessile serrated lesions and from those on the bowel cancer screening pathway or those with inflammatory bowel disease undergoing colonoscopy.

For healthy controls, fully anonymised blood samples were collected from the Oxford Biomedical Research Laboratory under The INForMeD Study (REC reference 16/LO/1376). All donors provided informed consent, and blood was drawn into EDTA-coated tubes. Healthy donor platelet apheresis samples were provided by Oxford NHS Blood and Transplant (NHSBT) through the Non-Clinical Issue (NCI) service.

The usage and collection of healthy human donor blood samples in Edinburgh was authorised under the project "21-EMREC-041 – The Role of Inflammation in Human Immunity". Freshly drawn blood from healthy human donors was collected into 50 ml BD Falcon tubes containing 4 ml of CPD buffer (16 mM citric acid, 90 mM sodium citrate, 16 mM NaH_2PO_4, 142 mM dextrose, pH 7.4).

For obstetric samples, 10 ml of blood was collected from mothers at the time of delivery, and postnatally at 24 and 48 hours after delivery into Streck blood collection tubes. Samples were taken at the Department of Women's and Reproductive Health at the John Radcliffe Hospital Oxford and approved by the Oxfordshire Research Ethics Committee (07/H0607/74). Sex of the neonate was confirmed after delivery and all mothers provided written informed consent.

Patients with immune thrombocytopenic purpura (ITP) were consented under the INForMeD Study (REC reference 16/LO/1376) and 10 ml of peripheral blood was collected into Streck tubes.

Animal models

All mice were bred and maintained in accordance with UK Home Office regulations. All experiments were performed under Project Licenses P2FF90EE8, P0B63BC4D and PP6460882 and approved by the University of Oxford Animal Welfare and Ethical Review Body. All mice were housed in individually ventilated cages at the animal unit either at Functional Genetics Facility (Wellcome Centre for Human Genetics, University of Oxford) or the Biomedical Services Facility at the John Radcliffe Hospital (The MRC Weatherall Institute of Molecular Medicine, University of Oxford), in a specific-pathogen-free (SPF) facility, with unrestricted access to food and water, and were not involved in any previous procedures.

For the immune thrombocytopenia model, CD45.2 female, wild-type mice were injected intra-venously with either an anti-platelet antibody to reduce platelet count (Emfret, cat # R300) or an IgG control that had no cytotoxic effects on platelets in mice (Emfret, cat # C301). Mice were humanely culled and blood collected via cardiac puncture into EDTA coated microvettes (Sarstedt, cat # 20.1288) at 24, 72 and 120 hours post treatment. Platelet counts were determined using an automated blood cell counter. cfDNA was extracted from plasma and quantified.

For the colorectal cancer (CRC) model, murine blood was drawn from KPN (*villin*Cre^{ER} *Kras*$^{G12D/+}$ *Trp53*$^{fl/fl}$ *R26*$^{N1icd/+}$) and KP (*villin*Cre^{ER} *Kras*$^{G12D/+}$ *Trp53*$^{fl/fl}$) mice via cardiac puncture into EDTA coated microvettes (Sarstedt, cat # 20.1288). All strains used in this model were maintained on C57BL/6J background. Both male and female KP and KPN mice were used.

For the orthotopic pancreatic cancer model, a total of 500 KPC-F cells (passages 9-11) were injected in a volume of 10 µl in a mixture of 50% Matrigel and 50% DMEM (Gibco) using a 0.5 ml Micro-fine insulin syringe (BD). Following anesthesia of the mice using 4% isoflurane/oxygen and clipping of hair, an incision of 1 cm was made in the left abdominal site. The spleen and pancreas were exteriorized using forceps and KPC-F cells were injected in the tail of the pancreas. Successful injection was verified by the appearance of a wheal at the injection site with no leakage through the pancreatic capsule. Spleen and pancreas were gently moved back into the peritoneal cavity; the abdominal wall was sutured with absorbable 4.0 Vicryl suture (Ethicon) and the skin was closed using a 7 mm wound clip. Two weeks post-surgery, after the mice had recovered, blood was drawn via cardiac puncture into EDTA-coated microtainer tubes (BD).

For the cohort of KPC mice treated with aspirin, aspirin (NSC 27223; Selleck Chemicals, cat #. S3017) was administered via intraperitoneal injection on alternate days at a dose of 10 mg/kg. Treatment began on day 4 after tumor cell implantation and continued every other day until day 14. Control animals received intraperitoneal injections of vehicle (2% DMSO in PBS) on the same schedule.

Blood cell isolation and nucleic acid extraction

Blood tubes were kept at room temperature and handled gently to avoid platelet activation. For human samples, platelets were isolated within 4 or 24 hours of blood sampling (depending on blood tube) using a modified previously published protocol(*3*). Briefly, whole blood was supplemented with citrate-dextrose solution (ACD) (Sigma Aldrich, cat # C3821-50ML) and centrifuged at 180 x g for 20 minutes at room temperature. Eighty % of the supernatant was removed using a Pasteur pipette, diluted with platelet wash buffer and centrifuged at 600 x g for 20 minutes at room temperature. The resulting platelet pellet was resuspended in pre-warmed HEPES-modified Tyrode's buffer. The remaining platelet poor plasma was centrifuged at 16'000 x g for 10 minutes at 4°C to ensure the pelleting of all cellular components and the isolation of pure plasma cfDNA. For the collection of platelets from healthy donor platelet apheresis bags, samples were pelleted at 600 x g for 20 minutes at room temperature. Platelet numbers were determined using an automated blood cell counter (Horiba, Pentra ES 60 Cell Counter).

Human mononuclear cells (MNCs) were isolated from freshly drawn venous blood into EDTA coated tubes. Whole blood was supplemented with ACD and centrifuged at 180 x g for 20 minutes at room temperature. The supernatant was removed and the remaining layer diluted with wash buffer (PBS pH 7.4 0.5% FBS, 2mM EDTA). Diluted blood was layered onto density gradient media (GE Healthcare, cat # 5442-03) and centrifuged for 20 minutes at 600 x g, low brake. MNCs were collected from the white inter-phase 'buffy coat' using a Pasteur pipette and transferred to a Falcon tube. Human red blood cells (RBCs) were sampled from the upper layer of the RBC/granulocyte pellet and diluted with wash buffer. The remaining RBC/granulocyte pellet was resuspended with chilled RBC Lysis Buffer (eBioscience, cat # 00-4300-54) and incubated at 4°C

for 5 minutes. The lysed sample was centrifuged at 1000 x g for 5 minutes, the supernatant discarded and the granulocyte pellet diluted with wash buffer. The remaining white granulocyte pellet was washed, centrifuged and stored at -80°C until required. Purity studies using an automated cell counter provided no evidence of MNC or RBC contamination in the granulocyte pellet.

DNA was extracted from equal volumes of fresh platelets (resuspended in HEPES-modified Tyrode's buffer) and 'platelet poor plasma' using the QIAamp cfDNA kit (Qiagen, cat # 55114), as per the manufacturer's instructions. Genomic DNA was extracted from nucleated cells using the DNeasy Blood & Tissue Kit (Qiagen, cat # 51104). Extracted DNA was quantified using a Qubit fluorometer (Thermofisher Scientific) and stored at -80°C until required.

Mouse platelets were isolated within four hours of blood collection via cardiac puncture. Whole blood was supplemented with ACD and centrifuged at 100 x g for 10 minutes at room temperature. The plasma was removed and collected into a 1.5 ml Eppendorf tube. The plasma was then diluted with platelet wash buffer and centrifuged at 3500 x g for 11 minutes to pellet the platelets. The platelet pellet was resuspended in pre-warmed HEPES-modified Tyrode's buffer. The platelet poor plasma was removed and centrifuged at 1300 to 16'000 x g for 10 minutes at 4°C to remove all cells and debris, and the final supernatant collected for cfDNA isolation.

Cell lines

The following cancer cell lines were used as positive and negative controls for common cancer-associated mutations; HCT116 (CVCL S744) *PIK3CA*H1047R, LS180 (CVCL 0397) *KRAS*G12D, COLO205 (CVCL 0218) *BRAF*V600E, HEL (CVCL_0001) *JAK2*V617F. All cell lines were purchased from American Type Culture Collection (cat # CCL-247, CL-187, CCL-222 and TIB-180 for HCT116, LS180, COLO205 and HEL cells respectively). All cells were cultured according to American Type Culture Collection recommendations and tested monthly for mycoplasma contamination.

NKPCB-NBC12.1F (KPC-F) cells, derived from a KPC mouse (LSL-*Kras*G12D; LSL-*Trp53*R172H; *Pdx1*Cre) were cultured in DMEM (Gibco) supplemented with 10% FBS, 2 mM glutamine, 100 U/ ml penicillin, 100 µg/ ml streptomycin and maintained under at 37 °C with 5% CO_2.

The human Burkitt's lymphoma cell line, BL2 (CVCL 1966, cat # CRL-2959) was used to generate tumor cell-derived extracellular vesicles (EVs). Both standard BL2 cells and BL2 cells stably transfected with the apoptosis-suppressing gene *BCL2* were used, to obtain apoptotic (apo-EVs) from BL2 cells and non-apoptotic EVs (non-apo-EVs) from apoptosis-resistant BL2-Bcl-2 cells. Protein expression was regularly tested by flow cytometry, confirming that 98% of the BL2-Bcl-2 cells expressed BCL2. Both cell lines were maintained in 50% X-VIVO medium (50% Gibco RPMI-1640, 50% X-VIVO-20 medium; Lonza, Basel, Switzerland), supplemented with 50 U/ml penicillin and 50 µg/ml streptomycin at 37 °C with 5% CO_2.

Generation of extracellular vesicles (EVs) from BL2 and BL2-Bcl-2 cells

BL2 and BL2-Bcl-2 cells were cultured at 20 x 10^6/ml in 0.1 µm filtered 50% X-vivo 20 and irradiated with ultraviolet light to induce apoptosis with 6 doses at 50mJ/cm^2, for a total of 300mJ/cm^2. Apoptosis was monitored hourly by Annexin V and Sytox Blue staining. To isolate EVs, the culture supernatant was centrifuged at 25 x g for 1 hour followed by sequential filtering through a 5 µm mesh filter and a 1.2 µm syringe filter.

Purification and labeling of apo- and non-apo EVs

The EVs were purified from soluble factors and proteins from the cell culture by size exclusion chromatography using in-house prepared sepharose columns (Thermofisher, cat # 45-000-067 and Sigma Aldrich, cat # CL6B200-100ML). After purification, EV concentration and size profile was measured by Nanoparticle Tracking Analysis using a NanoSight LM10 and Malvern NanoSight software (v3.3). The software analyzes each sample five times to give the average concentration, mean and modal size of each sample. EV size ranged between 150-200 nm and the concentration was between 100-200 x 10^8/ml. The number of EVs added to platelets was standardized across experiments, using a ratio of 50 x 10^8 EVs with 1 x 10^7 healthy donor platelets. For imaging experiments, prior to incubation with platelets, the purified EVs were suspended in 0.1 µm filtered HBSS and were stained with Biotium CF568 NHS ester with a covalent attachment of the dye to EV proteins, according to the manufacturer's protocol (Biotium, cat # NC1542764). To remove unbound dye, the EVs were purified again by size exclusion chromatography through sepharose columns.

Flow cytometry and fluorescence-activated cell sorting (FACS)

All experiments were carried out using an LSRFortessa X-20 flow cytometer (Becton, Dickinson and Company). Platelets and paired plasma were prepared as previously described, pelleted and resuspended in HEPES-modified Tyrode's buffer. The samples were stained with a cocktail of antibodies for 20 minutes at room temperature in the dark, prior to being washed and resuspended in fresh buffer for flow cytometric analysis. The antibodies used are as follows, CD42 FITC, CD41 PE-Cy7, CD3 PE, CD11b and CD33 APC, CD19 APC-Cy7 and CD235a BV650. To assess the nucleic acid content of platelets, healthy donor blood was drawn into EDTA-coated tubes and platelets were isolated as previously described. The platelets were stained with the antibody CD42 PeCy7 and nucleic acid stains DRAQ5 (DNA) and Syto-13 (RNA) for 20 minutes at room temperature in the dark. After incubation, the platelets were washed and resuspended in fresh HEPES-modified Tyrode's buffer for analysis. Compensation beads (were stained and analyzed in parallel, as an additional negative control to fluorescence minus one (FMO) controls to confirm no non-specific binding of the nucleic acid stains (BD Invitrogen, cat # 01-1111-42). To assess platelet activation, platelets were isolated from healthy donor blood drawn into citrate tubes. Following isolation, platelets were maintained at a physiological concentration of ~300 x 10^6 /ml.

To evaluate the activation status and DNA content of healthy donor platelets, after isolation, platelets were stained with CD42 FITC, and antibodies for activation; CD63 PB and CD62P BV857. The DNA content was simultaneously assessed by the inclusion of the DNA marker, DRAQ5. After a 20-minute incubation at room temperature, the platelets were washed and resuspended in HEPES-modified Tyrode's buffer.

To determine changes in platelet DNA content upon activation, 10 µl of platelets were added to Eppendorf tubes containing the antibodies CD42 FITC, CD63 PB and CD62P BV857 and the DNA stain DRAQ5. The platelets were then treated with 3 µl of either a 'resting' or an 'activation' buffer, both comprising HEPES-modified Tyrode's buffer supplemented with 20 mM calcium (Sigma-Aldrich, cat. # 21115-100ML). For the activation buffer, the agonist TRAP-6 was added at concentrations of 5, 10, 50, or 100 µM (10x the final concentration, Bachem AG, cat. # 4031274.0025). After a 15-minute incubation at room temperature, the platelets were washed twice prior to resuspension in HEPES-modified Tyrode's buffer and analyzed.

The BD FACSymphony S6 was used for cell sorting. 30 µl of healthy donor blood was diluted with an antibody cocktail to a final volume of 100 µl. The platelets were incubated for 20 minutes at room temperature in the dark, washed and resuspended in fresh buffer. The staining solution included the following antibodies, CD42 FITC, CD3 BV421, CD11b and CD33 APC, CD19 APC-Cy7 and CD235a FITC. Platelets ($CD42^+$, $CD3^-$, $CD11b^-$, $CD33^-$, $CD19^-$ and $CD235a^-$) were sorted into 15 ml falcon tubes containing HEPES-modified Tyrode's buffer. The platelets were centrifuged at 600 x g for 20 minutes, the supernatant removed, and pellet frozen at -20°C.

Single color-stained controls and FMO controls were used for all experiments. FACS data were collected using BD FACSDiva software (v9.0) and gates were set using FMO controls and negative populations. All antibodies and nucleic acid stains are listed in table S7.

Droplet Digital PCR (ddPCR)

ddPCR assays were ordered from Bio-Rad. All ddPCR assays were conducted on a QX200 Droplet Digital PCR System using the manufacturer's recommended protocol and reagents (Bio-Rad Laboratories). Positive and negative controls were included in every assay. Analysis was performed using the QuantaSoft software (Bio-Rad Laboratories, Watford UK).

To detect mouse *KRAS*G12D, a ddPCR assay was designed for the detection of the *KRAS* p.G12D c.35G>A point mutation. Primers for the detection of *KRAS* were as follows: forward 5'-GCCTGCTGAAAATGACTGAG-3' and reverse 5'-CGTAGGGTCATACTCATCCAC-3'. Two dual labeled probes were also used to target the wild-type and mutant sequences.
Wild-type 5'-HEX- ACGCC[+A][+C]CAG[+C]TCCAA-BHQ1-3' and mutant 5'-6FAM-AC[+G]CC[+A][+T][+C]AG[+C]TCCAA-BHQ1-3'. Square brackets indicate LNA bases (Merck Life Sciences).

Synthetic DNA oligo generation

Single stranded DNA oligos were designed to include the mouse *KRAS*G12D genetic marker and synthesized by Integrated DNA Technologies (IDT, Iowa USA). Synthesized DNA was reconstituted according to the manufacturers protocol. PCR assays for the detection of *KRAS* were performed using the KAPA2G Fast HotStart PCR Kit (Roche, cat # KK5512) and primers were as follows: forward 5'-GCCTGCTGAAAATGACTGAG-3' and reverse 5'-CGTAGGGTCATACTCATCCAC-3'. Fragmentation profiles of DNA oligos were analyzed using an Agilent Tapestation 2200 system (Agilent Technologies). Electrophoresis data was analyzed using the Tapestation Analysis Software (Agilent).

In vitro co-culture of platelets, tumor cells, EVs, and synthetic DNA oligos

To explore uptake of DNA shed from tumor cells, platelets (3 x 10^5 /µl), MNCs (0.075 x 10^5/µl) and RBCs (3 x 10^5 /µl) from healthy donors were added to individual wells within a 24-well plate and a 1.0 µm TC Insert (Sartstedt, cat # 83.3932.101) placed into the well. Cancer cells (0.03 x 10^5/µl) were carefully placed in the inserts and the plate incubated for approximately eight hours at 37°C. Control samples were incubated simultaneously but without the addition of tumor cells. After incubation, the inserts were removed and the blood cells transferred to Eppendorfs. To ensure complete removal of any contaminating cfDNA in the media, all cells/platelets were washed and centrifuged at 600 x g for 10 minutes. The supernatant was removed and the pelleted blood cells re-suspended in fresh buffer. The cells were washed for a total of three times and finally resuspended in 1 ml of fresh pre-warmed HEPES-modified Tyrode's buffer prior to DNA extraction using the QIAamp cfDNA kit. Following DNA extraction, the samples were quantified and ddPCR was used to identify the presence of mutant alleles.

To investigate platelet uptake of DNA containing EVs, 50 x 10^8 labelled, purified apo- and non-apo EVs resuspended in in Tyrode's buffer were incubated with 0.1x 10^8 platelets for three hours at 37°C with gentle inversion every 30 minutes. Following incubation, the samples were centrifuged for 20 minutes at 800 x g. The supernatant was discarded, and the platelets re-suspended in 300 µl of PBS. EV and platelet pellets were treated with DNase as per manufacturer's protocol (Sigma Aldrich, cat # AMPD1) and then DNA extracted using the QIAamp cfDNA kit. Following DNA extraction, the samples were quantified and assayed for the male *SRY* gene using ddPCR.

To understand whether platelets also take up 'free' DNA fragments, platelets were incubated with synthetic DNA fragments ranging from 128-657 bp. Healthy donor human platelets were aliquoted into Eppendorf tubes and spiked with reconstituted synthetic DNA oligos for a final concentration of 10 ng/ml. The platelets were mixed gently by pipetting and incubated at 37°C overnight. Following incubation, the platelets were centrifuged for 10 minutes at 600 x g. The supernatant (containing excess DNA oligo) was discarded, and the platelets re-suspended in fresh buffer. The platelets were washed for a total of two times and finally resuspended in 1ml of fresh pre-warmed HEPES-modified Tyrode's buffer prior to DNA extraction using the QIAamp cfDNA kit. Eluted DNA was PCR amplified using the KAPA2G Fast HotStart PCR Kit (Roche, cat # KK5512) and fragment length was confirmed using the Agilent Tapestation.

DNase treatment to investigate platelet DNA internalization

Platelets were incubated with HEL erythroleukemia cells as previously described. Following co-incubation, platelets were treated with DNase according to the manufacturers protocol (Ambion DNA-free Kit, cat # AM1906). To confirm catalytic activity of the enzyme, DNase was also added to conditioned media. Following DNase treatment, the platelet samples were washed with 500 µl of 5mM EDTA and centrifuged at 600 x g for 10 minutes. The supernatant was removed and the wash repeated. After the second centrifugation, the supernatant was discarded and the platelet pellet resuspended in 1 ml of fresh pre-warmed HEPES-modified Tyrode's buffer. Following DNase inactivation of the conditioned media, 900 µl of HEPES buffer was added to a final volume of 1 ml in preparation for DNA extraction. For control samples, no DNase was added and 10 µl of 1M tris-HCL was added in replacement of 10X DNase I Buffer for the platelet samples.

In a separate experiment, healthy donor platelets or an equal volume of HEPES-modified Tyrode's buffer (to mimic plasma) was spiked with a 260 bp synthetic DNA oligo and incubated overnight. The samples were then treated with DNase according to the manufacturers protocol (Life technologies, RapidOut DNA Removal Kit, cat # K2981). Following DNase treatment, the platelet samples were washed and centrifuged at 600 x g for 10 minutes. The supernatant was removed and platelet pellet wash repeated. After the second centrifugation, the supernatant was discarded and the platelet pellet resuspended in 1 ml of fresh pre-warmed HEPES-modified Tyrode's buffer. For 'cfDNA' (buffer) samples, DNase was inactivated and 900 µl of HEPES buffer was added to a final volume of 1 ml. DNA was extracted from all samples using the QIAamp cfDNA kit. Eluted DNA was PCR amplified and the fragment length confirmed as previously described. For control samples, no DNase was added and 10 µl of 1M tris-HCL was added in replacement of 10X DNase I Buffer for the platelet samples.

Inhibition of cargo-trafficking by platelets

Healthy donor human platelets were treated with the following inhibitors or appropriate negative control molecules; Dynole 34-2 (Abcam, cat # ab120463, 30 µM), Dynole 31-2, Negative control (Abcam, cat # ab120464-5mg, 30 µM), Pitstop (Abcam, cat # ab120687, 25 µM), Pitstop 2 Negative control, (Abcam, cat # ab120688, 25 µM), Cytochalasin D (Santa Cruz Biotechnology, cat # CAS 22144-77-0, 5 µM), Nystatin (Merck Life Science UK, cat # N9150-20ML, 30 units/ml), Amiloride (Abcam cat # ab120281, 500 µM), Imipramine (Abcam, cat # ab141046, 5 µM). After treatment, platelets were spiked with a 260 bp synthetic DNA oligo for a final concentration of 10 ng/ml and incubated at 37°C overnight. Following incubation, the platelets were centrifuged for 10 minutes at 600 x g. The supernatant (containing excess inhibitor/ negative control and DNA oligo) was discarded, and the platelets re-suspended in fresh buffer. The platelets were washed for a total of two times and finally resuspended in 1 ml of fresh pre-warmed HEPES-modified Tyrode's buffer prior to DNA extraction using the QIAamp cfDNA kit. Eluted DNA was PCR amplified and the fragment length confirmed as previously described.

To assess the impact of platelet activation inhibition on platelet DNA uptake, platelets were treated with 500, 1000 or 2000 µM aspirin (Merck Life Sciences, cat # A2093-500G) or 5, 50, 100 or 200 µM Ibrutinib (PCI-32765) (Stratech Scientific Ltd, cat # S2680-SEL-5mg). Following treatment, a 260 or 367 bp synthetic DNA oligo was added to resting platelets for a final concentration of 10 ng/ml DNA and incubated at 37°C overnight. Following incubation, the platelets were centrifuged for 10 minutes at 600 x g. The supernatant (containing excess inhibitor/ negative control and DNA oligo) was discarded, and the platelets re-suspended in fresh buffer. The platelets were washed for a total of two times and finally resuspended in 1 ml of fresh pre-warmed HEPES-modified Tyrode's buffer prior to DNA extraction. Eluted DNA was amplified by PCR and the Agilent TapeStation was used to confirm fragment length.

To assess the impact of dynamin inhibition on platelet secretion, platelets were treated with Dynole or paired negative control, exposed to the 260 bp synthetic DNA oligo and incubated overnight. Following incubation, the platelets were pelleted, resuspended in fresh buffer, re-treated with the inhibitor or negative control and incubated for 3 hours at 37°C. After the second incubation, the platelets were pelleted and discarded, and the supernatant (platelet 'releasate')

was collected. The supernatant was centrifuged at 16'000 x g for 5 minutes to ensure complete removal of any contaminating platelets and subject to DNA extraction, PCR amplification and fragment analysis.

To understand the impact of dynamin inhibition on platelet EV internalization, 0.1x 10^8 healthy donor platelets were incubated with either the dynamin inhibitor, paired negative control or DMSO for 30 minutes at 37°C. After incubation, 50 x 10^8 labelled, purified apo-EVs re-suspended in Tyrode's buffer were added to the treated platelets and incubated as previously described prior to DNase treatment, DNA extraction and *SRY* ddPCR.

H3k27ac ChIPmentation of platelet chromatin

Platelets were isolated from plateletpheresis samples from 3 independent healthy donors. 13 ml of each sample was centrifuged at 600 x g for 30 minutes at room temperature, the supernatant was removed and platelet pellets were immediately used for H3K27ac ChIPmentation using a protocol tailored for low-DNA input samples from a published protocol(*65*), using the H3k27ac antibody (Diagenode, cat # C15410196). In brief, bead-bound chromatin undergoes a one-step adaptor insertion via Tn5 tagmentation and only one post-PCR DNA purification is performed to reduce sample loss.

For each reaction, 5 µl A-Dynabeads (Invitrogen cat # 10001D) were coated with the H3K27ac antibody (Diagenode, cat # C15410196) (150 µl PBS, 0.5% BSA, 1x Proteinase inhibitor). The antibody-bound beads were then washed in PBS and 0.5% FBS, before being added to samples for overnight incubation.

Platelet pellets were incubated in 600 µl lysis buffer (50 mM Tris pH 8, 10 mM EDTA, 0.5% SDS, 1x Protease Inhibitor) for 20 minutes on ice. Then, 1% Triton-X100 was added, and the samples centrifuged to pellet insoluble material. The supernatant was split into three 200 µl sub-samples, and the samples were incubated overnight with the H3k27ac antibody coated beads. Before incubation, 5% of the sample was kept aside for input control tagmentation.

After overnight incubation, the beads were washed three times with RIPA wash buffer (50 mM HEPES pH 7.6, 500 mM LiCl1, 1 mM EDTA, 1% NP-40 / IGEPAL CA-630, 0.7% Na-Deoxycholate), followed by one wash with TE and then 10 mM Tris pH8. Beads and input control samples were then tagmented in tagmentation buffer (50 mM Tris pH 8, 25 mM MgCl2, 50% Dimethylformamide) with Tn5 transposase (Illumina, cat # 20034197) for 10 minutes at 37°C and immediately cooled down. Beads were immediately washed. Library preparation was then conducted with Nextera-based sequencing primers(*66*). qPCR and fragmentation analysis were performed.

Immunofluorescence microscopy

Live

To visualize platelet DNA uptake *in vitro*, washed human platelets were stained with anti-CD42 AF488 (BioLegend, cat # 303914) for 30 minutes at room temperature. Separately, COLO205 cells or H2B-mCherry HEL cells were labeled using either the highly specific live cell DNA stain, SiR-DNA (Spirochrome, cat # CHF260.00), NUCLEAR-ID Red DNA stain or DAPI (HEL only) as

per the manufactures' protocols (Enzo Life Sciences, cat # ENZ-52406). Stained COLO205 or H2B-mCherry HEL cells were then washed and added to collagen type-1 (Corning, cat # 354236)-coated microscopy slides (Greiner Bio-One, cat # 543079). CD42 stained platelets were added to the wells containing tumor cells immediately before imaging. To analyze endogenous wild-type DNA within healthy donor platelets, platelets were co-stained with anti-CD42 AF488 and NUCLEAR-ID Red DNA and imaged alone.

Regarding platelet uptake of tumor derived DNA from conditioned media, COLO205 cells were labeled with NUCLEAR-ID Red. Following staining, the cells were washed with MEM Alpha 5% FCS, pelleted and the supernatant removed. The cells were washed a further two times to ensure complete removal of the DNA stain and resuspended in 200 µl of fresh media. The cells were incubated at 37°C and vortexed periodically to encourage cell death and DNA release. After two hours, the COLO205 cells were centrifuged at 16'000 x g for 10 minutes at 4°C. Supernatant was removed from the pelleted cells, transferred to a fresh Eppendorf and the cell pellet discarded. Healthy donor platelets were stained with anti-CD42 AF488 and added to wells of Poly-L-lysine coated slides (Ibidi, cat # 81201). DNA labeled COLO205 cell conditioned media was added to the platelets immediately before imaging. All live imaging was performed using the Zeiss Spinning Disk Confocal with a 63X oil immersion objective.

Fixed

BL2 cell-derived apo-EVs were isolated, labeled with an amine-reactive fluorescent dye (Biotium, cat # 92131) and frozen as previously described. Prior to imaging, the EVs were thawed and co-stained with DAPI for 30 minutes at room temperature. The EVs were washed twice, pelleted at 20'000 x g for 30 minutes at 4°C and resuspended in HBSS buffer. Labeled EVs were then added to Poly-L-lysine coated chamber slides and incubated overnight at 4°C. Following incubation, the supernatant was carefully removed and the EVs fixed with 4% formaldehyde at room temperature for 30 minutes. The fixative was then removed and the EVs gently washed three times with PBS. To confirm imaging of EVs and not auto-fluorescent debris, PBS was stained with DAPI, incubated overnight, and fixed onto slides alongside the EV preparations. The slides were mounted and the EVs and PBS controls resolved by fluorescence microscopy using a Zeiss LSM900 with a 63X oil immersion objective.

To visualize platelet sequestration of EVs, 5 x 10^9 apo-EVs labeled with an amine-reactive fluorescent dye were thawed and added to 1 ml of 10 x 10^6 washed healthy donor platelets and incubated for three hours at 37°C. To ensure adequate mixing, the cells were inverted gently every 30 minutes. Following incubation, the cells were centrifuged at 800 x g for 20 minutes, low brake. The supernatant (containing the EVs) was removed, and the platelets resuspended in PBS. Platelets were centrifuged onto a Poly-L-lysine coated chamber slide at 600 x g for 20 minutes and fixed in 2% formaldehyde/PBS for 10 minutes at room temperature. The fixative was removed and the platelets washed twice with PBS. The platelets were then labeled with anti-CD42 AF488 for 20 minutes at room temperature. After labeling, the slides were washed, mounted with ProLong Gold Antifade Mountant (Thermofisher, cat # P36930) and imaged using the Zeiss LSM900.

Histology, immunohistochemistry, and imaging of peripheral blood films

Cell contamination was assessed after cytospin of the resuspended platelet pellet onto a glass slide (5 minutes at 500 r.pm.) and May–Grünwald Giemsa staining, according to standard protocols. Images were obtained using an Olympus BX60 Microscope.

KPC mice were sacrificed, and pancreatic tissue was taken for p53 immunohistochemical staining. Briefly, a total of 24 hours post fixation in 10% neutral buffered formalin at 4°C, tissues were transferred to 70% ethanol and stored overnight at 4°C. Fixed tissues were processed overnight using the STP120 Spin Tissue Processor (Thermo Fisher Scientific) and embedded the next day in paraffin wax. Tissues were cut into 4 µm sections using a Leica RM215 microtome and adhered onto SuperFrost Ultra Plus Adhesion slides (Thermo Fisher Scientific) before drying overnight in a 37°C incubator. After deparaffinization, rehydration in an ethanol gradient (100%, 70%, 50%), and antigen retrieval with Citrate Buffer Antigen Retriever (Sigma-Aldrich), slides were incubated with Dual Endogenous Enzyme-Blocking Reagent (Dako) for 1 hour, washed in PBS, incubated with 5% goat serum for 30 minutes, washed in PBS again, and incubated with the primary antibody, p53 (Cell Signaling Technologies, cat # 2524) diluted 1:2000 for 2 hours at room temperature. Slides were then washed in PBS with 0.05% Polysorbate 20 and incubated with the secondary antibody, horse anti-mouse IgG (Cell Signaling Technologies, cat # 7076), diluted 1:100 for 45 minutes at room temperature, washed in PBS with 0.05% Polysorbate 20 again, and incubated with 3,3′-Diaminobenzidine (DAB) chromogen for 3 minutes at room temperature. After staining, slides were dehydrated in an ethanol gradient (50% 70%, 100%), followed by tissue clearing in xylene (ThermoFisher). Slides were mounted with dibutylphthalate polystyrene xylene (DPX; Sigma-Aldrich), dried for 24 hours and scanned using an Aperio ScanScope CS digital slide scanner (Leica Biosystems) at 20X magnification.

Healthy donor blood was used to prepare a peripheral blood film. The blood smear was fixed with 100% methanol for 30 seconds and stained with CD42 AF488 (BioLegend, cat # 303914) to identify platelets and the DNA stain Hoechst (Invitrogen, cat # H3570), to identify nucleated cells. The slide was mounted with a coverslip and imaged using the Leica SPE.

Fluorescence In Situ Hybridization (FISH)

Platelets in suspension were centrifuged onto Poly-L-lysine coated chamber slides and fixed in 2% formaldehyde/PBS for 10 minutes at room temperature. The platelets were then permeabilized in 0.5% Triton X-100/PBS for 10 minutes at room temperature and washed twice in 0.05% Triton-X 100/PBS. The platelets were washed in 0.02% Tween20/PBS (PBST) and incubated with the primary anti-β-tubulin antibody (Sigma Aldrich, cat # T5201) diluted in blocking buffer for 30 minutes at 37ºC in a humid box. Following primary labeling, the platelets were washed with PBST and incubated with the secondary donkey anti-mouse IgG H&L AF405 antibody (Abcam, cat # ab175658) diluted in blocking buffer for 30 minutes at 37ºC. The labeled platelets were then washed with PBST, fixed and washed with PBS for 10 minutes at room temperature. FISH staining was carried out according to the manufacturer's protocol. Briefly, slides were incubated in 0.1N HCL, washed with 2x SSC and dehydrated in 70% ethanol for 3 minutes. Equal volumes of X- and Y-chromosome probes (Metasystems, cat # D-0323-050-FI and D-0324-100-OR) were added to the slide and covered with a 22 x 22 mm^2 coverslip. The slides were incubated at 85ºC for 5 minutes, sealed with rubber cement and incubated in a humidified chamber at 37°C overnight. Following hybridization, the rubber seal was removed, and

the slides washed in 0.1x SSC at 60ºC. Slides were mounted and imaged using the Zeiss LSM900 with a 63X oil immersion objective. Control cells (HEL cells and MNCs) were fixed onto slides, permeabilized and labeled with the X- and Y- chromosome paints. Following overnight hybridization, the cells were washed and counterstained with DAPI.

Airyscan imaging of platelet ultrastructure

Glass coverslips (VWR, cat # 631-0150) were coated with 5 µg/ml fibrillar collagen-I (Horm), (Nycomed) and incubated at 4ºC overnight in a 24 well plate. The coverslips were blocked with 5 mg/ml BSA for 1 hour at room temperature. After blocking, the BSA was removed and 300 µl of washed healthy donor platelets diluted to $1x10^7$/ ml was added to the wells. The platelets were left to spread for 45 minutes in a humidified chamber at 37°C. Following incubation, the liquid was carefully removed and washed with PBS. The platelets were fixed with 5% formalin for 10 minutes at room temperature, washed with PBS and permeabilized with 0.1% Triton-X 100/PBS (Sigma, cat # SLCF5969) for 5 minutes. The slides were washed with PBS and blocked for 30 minutes with blocking buffer (1% BSA + 2% goat + 2% donkey serum). The primary antibodies: mouse anti- human CD63, mouse anti- human LAMP2, rabbit anti- human TOM20, rabbit anti- human CD81 and mouse anti- human CD62P were diluted in blocking buffer and incubated with the platelets at 4ºC overnight. Following primary incubation, the coverslips were washed three times with PBS and incubated with the DNA stains (DRAQ5, NUCLEAR-ID Red, Hoechst) and the secondary antibodies; goat anti- mouse IgG H&L AF568 and goat anti- rabbit IgG H&L AF488 for 45 minutes at 37°C. Following incubation, the coverslips were washed and mounted onto imaging slides using Hydromount (Scientific Laboratory Supplies Ltd, cat # NAT1324). The slides were imaged using the Airyscan function of a Zeiss LSM 980 confocal microscope (63X objective lens, NA 1.4).

Quantitative analysis of imaging data and image analysis software

Images were analyzed using ImageJ (v2.1.0) (National Institute of Health, US-MD) and 3D reconstructions were generated in Imaris Viewer v9.7.0 (Oxford Instruments, Abingdon). CellProfiler (v4.0.7) (Broad Institute, US-MA) was used to quantitatively analyze platelet-tumor cell interaction. In brief, cells were segmented using the 'Identify Primary/Secondary Object' module. Thresholding strategies were employed to accurately mask cells for segmentation. Platelets were tracked using the 'Track Objects' module. Finally, AF647 intensity was measured using 'Measure Object Intensity' and data 'Exported to Spreadsheet'. This image-analysis pipeline, as well as others can be recreated in Cell Profiler tool (freely available from the Broad Institute at www.cellprofiler.org).

For co-localization analysis, we calculated the Pearson's correlation coefficient, r and Mander's overlap coefficient, *R* for each platelet by manually defining a cuboid region (90 x 90 pixels; 3.8 x 3.8 µm), enclosing fluorescence from all three channels. The equations used to calculate fluorescence correlation coefficients are described in the Supplementary Text, with calculations performed using MATLAB as described by Jung et al(*67*).

To assess the location of the DNA fluorescence within the platelet we developed a simple algorithm in MATLAB to calculate the total intensity of the DNA marker in a 3- dimensional (3D) platelet mask that was subsequently eroded away from the surface to the center. First, we generated a 3D platelet mask by applying a one level Otsu thresholding algorithm to the CD62P

fluorescence signal. The DNA intensity within the platelet was obtained by integrating the DRAQ5 fluorescence signal from pixels within the 3D platelet mask. To determine the position of the DNA fluorescence within the platelet, we used a series of one pixel erosion operations on the original 3D mask. After each erosion step, a convex hull was applied to ensure there were no 'holes' in the mask. The integrated DNA fluorescence intensity was then obtained within this new eroded mask. This procedure was repeated until a single pixel of the 3D platelet mask remained i.e. the center of the platelet had been reached.

Whole genome sequencing (WGS)

WGS was performed on paired pDNA and cfDNA isolated simultaneously from the same peripheral blood samples of 15 patients with a recent diagnosis of gastrointestinal adenocarcinoma. Libraries were prepared from samples that were confirmed (using the Agilent Tapestation) to have both short DNA fragments of approximately 160 bp in addition to longer peaks of ~12'000 bp. Long platelet DNA was fragmented prior to library preparation. Briefly, 15 µl of DNA diluted in TE buffer (1mM Tris-HCl, pH 8.0, 0.1 mM EDTA) was added to a Covaris microtube-15 (Covaris, cat # 520145) and briefly centrifuged at 3000 x g for 1 minute. The microtube was loaded onto the Covaris ME220 Focused-ultrasonicator and the protocol run using the treatment conditions required for a 150 bp target peak. Fragment size was determined using the Agilent Tapestation 2200 system (Agilent Technologies) and the sonication was repeated if DNA fragments were > 150 bp.

DNA-Seq libraries were prepared using the NEBNext Ultra II DNA Sample Preparation Kit for Illumina (New England BioLabs, Ipswich, MA, USA) according to the manufacturer's protocol. pDNA was size selected into 2 groups: short fragments (s-pDNA; under 600 bp) and long fragments (l-pDNA; over 600 bp). The short fragments were further cleaned to remove <100 bp fragments and large platelet fragments were fragmented via sonication as previously described. Following end repair and adapter ligation, adapter-ligated DNA fragments were amplified in enrichment PCR to generate final libraries. Cleaned up libraries were then multiplexed, and 1.5 pM libraries analyzed on an Illumina NextSeq 500 (300 cycle PE) at low-pass (0.1x) for all samples, and 10x for the cfDNA and s-pDNA, using four lanes in each sample with 4% PhiX to monitor sequencing performance. This amounted to 240 fastq files.

Data pre-processing

Quality control of all fastq files was conducted by running FastQC (v0.11.8)(*68*). Reads were adaptor- and quality-trimmed using Trim Galore!(*69*) (v0.6.5) and aligned to the GATK Genome Reference Consortium Human Build 38 (GRCh38)(*70*) using bwa-mem (v0.7.17)(*71*). Reads were aligned to alternate contigs to represent common complex variation using bwa_postalt.js (https://github.com/lh3/bwa/blob/master/bwakit/README.md)(*71*). Resulting BAM files were merged, sorted and indexed with samtools (v1.13.0)(*72*).

GATK toolkit (v4.1.7.0) was used to mark optical and PCR duplicates, estimate library complexity, and calculate summary metrics on insert sizes(*73*). Mapping rate was evaluated with samtools flagstat and the number of reads mapped to each chromosome and the mitochondrial genome with idxstats. Repetitive elements in the ENCODE blacklist(*74*) were excluded using bedtools intersect (v2.30.0)(*75*).

945

Insert size distribution

For all uniquely mapped, non-duplicated and properly paired read pairs, the frequency of insert size values was counted across all autosomes and chromosome X using samtools(*72*) and R. The distributions were plotted using ggplot2(*76*).

950

Read depth around transcription start sites

Transcription start sites were defined by refTSS (v3.3)(*77*). We used the nearest refTSS entry to the 5' coding sequence of all protein coding genes. Coverage per base in a 2 kilobase pair (kbp) region around each TSS was extracted with Rsamtools, counting only uniquely mapped, non-
955 duplicate, correctly paired reads with insert sizes between 150 and 170 bp ("mono-nucleosome") or between 280 and 350 bp ("di-nucleosome"). Peripheral blood mononuclear cell (PBMC) gene expression values were taken from Blueprint Epigenome experiment: EGAX00001327129 (http://dcc.blueprint-epigenome.eu/#/experiments/ERX1123729).
Briefly, genes with posterior mean estimates of transcripts per million > 15 were defined as "highly
960 expressed" in PBMC.

Di-nucleosome peak difference quantification

A chi-square test of independence was performed in R with a simulated p-value to examine the relation between DNA type (cfDNA and s-pDNA) and the proportion of di-nucleosome fragments.
965 We separated the fragments in (i) fragments below 250 bp representing mono-nucleosome fragments; and (ii) fragments above 250 bp representing di-nucleosome fragments. The proportion of di-nucleosome fragments was higher in s-pDNA than in cfDNA ($P < 0.0005$ in all samples).

970 ***Chromosome coverage***

Coverage was calculated using samtools bedcov, using a bed file of 10 kbp non-overlapping windows for all main chromosomes, but excluding reads with mapQ <1. Position with mappability (as defined by umap: https://bismap.hoffmanlab.org/) in the lowest 8 percentile were removed(*78*). The Coverage was then corrected for mappability and GC content bias using a
975 linear regression model and visualized with karyoplotR(*79*).

Gini index

After filtering for reads that are first in pair, uniquely mapped, mapped in proper pair, primary alignments, and non-duplicates, (samtools view parameters: -f 2 -F 3972 -q 1), we calculated the
980 coverage with samtools depth. Evenness of coverage was evaluated by calculating the Gini index(*80*) on the short pDNA and cfDNA's coverage, which was previously binned into adjacent 10 kbp bins.

ichorCNA

985 Copy number alterations in the 10X and low-pass WGS were evaluated using ichorCNA (v0.2.0)(*39*) (github: https://github.com/broadinstitute/ichorCNA/releases/tag/v0.2.0).

Tumor tissue DNA sequencing and analysis

DNA from resected tumor tissue and adjacent tumor-free colonic mucosa was extracted using the Monarch Genomic DNA Purification Kit (Monarch, cat # T3010S). For sequencing, gDNA was prepared as follows: 500 ng per sample at a concentration of 25 ng/µl. The tumor samples were sequenced at 75x and the normal samples at 30x by Novogene UK Ltd. The complete NextFlow pipeline for processing sequencing output to mutation calls is provided in the Zenodo code repository. Briefly, reads were trimmed using Trim Galore! (*69*) (v0.6.5), requiring >= 2bp adapter overlap and quality-trimming bases with Phred score below 20, and aligned against the complete hg38 genome, including alt alleles, using bwa-mem2 using default parameters. Mutations were called independently using Mutect2 (v4.1.7.0), Strelka (v2.9.10) and Octopus (v0.7.0). Mutations called by only one caller were excluded.

Estimation of observed and expected tumor fragments

99 sets of random single-base mutations, each matching the unique mutation count identified in the tumor tissue of patient CRC_012, were generated by sampling from all SNVs detected in any WGS-sequenced colorectal cancer from TCGA. Any SNV overlapping a SNP (dbSNP v155) with > 0.5% allele frequency in 1000Genomes, HapMap, dbGaP_PopFreq, GnomAD_exomes, TOPMED or GnomAD were excluded, as well as variants identified as SNPs in the non-cancer control sample for patient CRC_012. Together with the original CRC_012 mutation set, this amounted to 100 mutation sets. For each set, reads covering the mutation positions were extracted, excluding improperly paired reads or reads with mapQ < 25. Detection rate was then calculated by dividing the count of reads containing the variant allele (min base quality: 10) by the total number of reads covering the mutation sites. Positions that exhibited an allele fraction of > 20% in plasma or platelet derived DNA were excluded as potential SNPs. The likelihood of observing a detection rate as high or higher than that of CRC_012 tissue mutations in that patient's plasma and platelet-derived DNA was calculated using a normal distribution parameterized to the observed mean and standard deviation of detection rates for random mutation sets. Code and intermediate files are deposited in the publication's Zenodo repository.

TAPS sample preparation

Short (< 600 bp) and long (> 600 bp) platelet DNA was separated using 0.55X AMPure beads, followed by a 1.8X clean-up of the short platelet DNA. Genomic TAPS was carried out on long platelet DNA and cfDNA TAPS was carried out on short platelet DNA, as previously described(*45, 81*). Briefly, long platelet DNA was mixed with spike-ins of 0.1% CpG-methylated lambda phage DNA and 0.01% unmodified 2 kbp plasmid DNA and was sonicated and size-selected to 300-500 bp prior to library construction. Short platelet DNA was mixed with pre-fragmented spike-ins of the same ratio and used directly in library construction. DNA was ligated with KAPA Unique Dual-Indexed Adapter Kit using KAPA HyperPrep Kit according to the manufacturer's protocol. The ligated DNA was subjected to mTet1-mediated oxidation and borane reduction. Converted DNA was then amplified with short primers ordered from IDT (FW-5'-AATGATACGGCGACCACCGAGATCTACAC-3', RV-5'-CAAGCAGAAGACGGCATACGAGAT-3') using KAPA HiFi HotStart Uracil+ ReadyMix PCR Kit for four cycles according to the manufacturer's protocol. The PCR product was purified with AMPure XP beads. Finally, libraries were sequenced for 300 cycles in paired-end mode on the NextSeq 2000 with XLEAP-SBS chemistry P4 cartridge.

TAPS data processing and analysis

Raw sequencing reads were trimmed from adapter sequences and low-quality bases using Trim Galore!(*69*) (v0.6.5) and assessed for quality with FastQC(*68*) (v0.11.9). Reads were aligned to the reference genome using BWA-MEM2(71) (v2.2.1) and duplicates were marked with Picard(73) (gatk, v4.4.0.0). BAM files were indexed and merged using samtools(*72*) (v1.16.1). TAPS conversion efficiency and methylation bias were estimated by analyzing sequencing spike-ins. Methylation levels were called using rastair (v0.8.1).

Sample cellular deconvolution was performed using WGBStools and UXM deconv as described in Loyfer et al. (2023)(*46*). A custom cellular atlas was built using the Loyfer et al. (2023) pat files for B cells, T cells, NK (natural killer) cells, blood granulocytes, monocytes, erythrocyte progenitors, hepatocytes and vascular endothelium, and an in-house megakaryocyte TAPS dataset. Lymphoid (B cells, T cells, and NK cells) and Myeloid (blood granulocytes, monocytes and erythrocyte progenitors) cells contributions were summed for visualization purposes. All code is available in the Zenodo repository.

Code availability

Code used in these studies is available from Zenodo (*82*).

Statistical analysis

Parametric tests, such as the paired Student's *t* test, were used for comparisons within the same group when the data appeared normally distributed based on visual inspection. When data were paired but not normally distributed, nonparametric tests such as the Wilcoxon signed-rank test were applied. For comparisons between independent groups, the Mann-Whitney *U* test was used to assess statistical significance.

References and notes

1. C. Deppermann, P. Kubes, Start a fire, kill the bug: The role of platelets in inflammation and infection. *Innate Immun* **24**, 335-348 (2018).
2. J. N. Thon *et al.*, T granules in human platelets function in TLR9 organization and signaling. *J Cell Biol* **198**, 561-574 (2012).
3. M. Koupenova *et al.*, The role of platelets in mediating a response to human influenza infection. *Nat Commun* **10**, 1780 (2019).
4. M. Koupenova, J. E. Freedman, Platelets and Immunity: Going Viral. *Arterioscler Thromb Vasc Biol* **40**, 1605-1607 (2020).
5. M. Koupenova *et al.*, Pollen-derived RNAs Are Found in the Human Circulation. *iScience* **19**, 916-926 (2019).
6. R. J. A. Nilsson *et al.*, Blood platelets contain tumor-derived RNA biomarkers. *Blood* **118**, 3680-3683 (2011).
7. Z. Shen *et al.*, Platelet transcriptome identifies progressive markers and potential therapeutic targets in chronic myeloproliferative neoplasms. *Cell Rep Med* **2**, 100425 (2021).
8. M. G. Best *et al.*, RNA-Seq of Tumor-Educated Platelets Enables Blood-Based Pan-Cancer, Multiclass, and Molecular Pathway Cancer Diagnostics. *Cancer Cell* **28**, 666-676 (2015).

9. S. In 't Veld *et al.*, Detection and localization of early- and late-stage cancers using platelet RNA. *Cancer Cell* **40**, 999-1009 e1006 (2022).
10. C. Bettegowda *et al.*, Detection of circulating tumor DNA in early- and late-stage human malignancies. *Sci Transl Med* **6**, 224ra224 (2014).
11. A. J. Bronkhorst, V. Ungerer, S. Holdenrieder, The emerging role of cell-free DNA as a molecular marker for cancer management. *Biomol Detect Quantif* **17**, 100087 (2019).
12. S. Cristiano *et al.*, Genome-wide cell-free DNA fragmentation in patients with cancer. *Nature* **570**, 385-389 (2019).
13. A. Dasari *et al.*, ctDNA applications and integration in colorectal cancer: an NCI Colon and Rectal-Anal Task Forces whitepaper. *Nat Rev Clin Oncol* **17**, 757-770 (2020).
14. F. Diehl *et al.*, Circulating mutant DNA to assess tumor dynamics. *Nat Med* **14**, 985-990 (2008).
15. C. Fiala, E. P. Diamandis, Utility of circulating tumor DNA in cancer diagnostics with emphasis on early detection. *BMC Med* **16**, 166 (2018).
16. J. C. M. Wan *et al.*, Liquid biopsies come of age: towards implementation of circulating tumour DNA. *Nat Rev Cancer* **17**, 223-238 (2017).
17. Y. M. Lo *et al.*, Presence of fetal DNA in maternal plasma and serum. *Lancet* **350**, 485-487 (1997).
18. L. Hille *et al.*, Evaluation of an Alternative Staining Method Using SYTO 13 to Determine Reticulated Platelets. *Thromb Haemost* **119**, 779-785 (2019).
19. P. C. Armstrong *et al.*, Temporal in vivo platelet labeling in mice reveals age-dependent receptor expression and conservation of specific mRNAs. *Blood Adv* **6**, 6028-6038 (2022).
20. H. E. Allan *et al.*, Proteome and functional decline as platelets age in the circulation. *J Thromb Haemost* **19**, 3095-3112 (2021).
21. J. Moss *et al.*, Megakaryocyte- and erythroblast-specific cell-free DNA patterns in plasma and platelets reflect thrombopoiesis and erythropoiesis levels. *Nat Commun* **14**, 7542 (2023).
22. G. Escolar, E. Leistikow, J. G. White, The fate of the open canalicular system in surface and suspension-activated platelets. *Blood* **74**, 1983-1988 (1989).
23. L. Balaj *et al.*, Tumour microvesicles contain retrotransposon elements and amplified oncogene sequences. *Nat Commun* **2**, 180 (2011).
24. C. Kahlert *et al.*, Identification of double-stranded genomic DNA spanning all chromosomes with mutated KRAS and p53 DNA in the serum exosomes of patients with pancreatic cancer. *J Biol Chem* **289**, 3869-3875 (2014).
25. A. Takahashi *et al.*, Exosomes maintain cellular homeostasis by excreting harmful DNA from cells. *Nat Commun* **8**, 15287 (2017).
26. Z. Hu, H. Chen, Y. Long, P. Li, Y. Gu, The main sources of circulating cell-free DNA: Apoptosis, necrosis and active secretion. *Crit Rev Oncol Hematol* **157**, 103166 (2021).
27. B. K. Thakur *et al.*, Double-stranded DNA in exosomes: a novel biomarker in cancer detection. *Cell Res* **24**, 766-769 (2014).
28. D. Jerez-Dolz *et al.*, Internalization of microparticles by platelets is partially mediated by toll-like receptor 4 and enhances platelet thrombogenicity. *Atherosclerosis* **294**, 17-24 (2020).
29. R. J. Nilsson *et al.*, Rearranged EML4-ALK fusion transcripts sequester in circulating blood platelets and enable blood-based crizotinib response monitoring in non-small-cell lung cancer. *Oncotarget* **7**, 1066-1075 (2016).

30. S. Koseoglu *et al.*, Dynamin-related protein-1 controls fusion pore dynamics during platelet granule exocytosis. *Arterioscler Thromb Vasc Biol* **33**, 481-488 (2013).
31. Y. Yatomi *et al.*, Separable function of platelet release reaction and clot retraction. *Biochem Biophys Res Commun* **140**, 329-334 (1986).
32. H. Melchinger, K. Jain, T. Tyagi, J. Hwa, Role of Platelet Mitochondria: Life in a Nucleus-Free Zone. *Front Cardiovasc Med* **6**, 153 (2019).
33. L. H. Boudreau *et al.*, Platelets release mitochondria serving as substrate for bactericidal group IIA-secreted phospholipase A2 to promote inflammation. *Blood* **124**, 2173-2183 (2014).
34. S. O'Hagan, M. Wright Muelas, P. J. Day, E. Lundberg, D. B. Kell, GeneGini: Assessment via the Gini Coefficient of Reference "Housekeeping" Genes and Diverse Human Transporter Expression Profiles. *Cell Syst* **6**, 230-244 e231 (2018).
35. M. W. Snyder, M. Kircher, A. J. Hill, R. M. Daza, J. Shendure, Cell-free DNA Comprises an In Vivo Nucleosome Footprint that Informs Its Tissues-Of-Origin. *Cell* **164**, 57-68 (2016).
36. F. Mouliere *et al.*, Enhanced detection of circulating tumor DNA by fragment size analysis. *Sci Transl Med* **10**, (2018).
37. H. R. Underhill *et al.*, Fragment Length of Circulating Tumor DNA. *PLoS Genet* **12**, e1006162 (2016).
38. Y. D. Lo, D. S. Han, P. Jiang, R. W. Chiu, Epigenetics, fragmentomics, and topology of cell-free DNA in liquid biopsies. *Science* **372**, eaaw3616 (2021).
39. V. A. Adalsteinsson *et al.*, Scalable whole-exome sequencing of cell-free DNA reveals high concordance with metastatic tumors. *Nat Commun* **8**, 1324 (2017).
40. C. Kandoth *et al.*, Mutational landscape and significance across 12 major cancer types. *Nature* **502**, 333-339 (2013).
41. A. Jamshidi *et al.*, Evaluation of cell-free DNA approaches for multi-cancer early detection. *Cancer Cell* **40**, 1537-1549 e1512 (2022).
42. M. S. Esfahani *et al.*, Inferring gene expression from cell-free DNA fragmentation profiles. *Nat Biotechnol* **40**, 585-597 (2022).
43. J. Moss *et al.*, Comprehensive human cell-type methylation atlas reveals origins of circulating cell-free DNA in health and disease. *Nat Commun* **9**, 5068 (2018).
44. R. Sadeh *et al.*, ChIP-seq of plasma cell-free nucleosomes identifies gene expression programs of the cells of origin. *Nat Biotechnol* **39**, 586-598 (2021).
45. Y. Liu *et al.*, Bisulfite-free direct detection of 5-methylcytosine and 5-hydroxymethylcytosine at base resolution. *Nat Biotechnol* **37**, 424-429 (2019).
46. N. Loyfer *et al.*, A DNA methylation atlas of normal human cell types. *Nature* **613**, 355-364 (2023).
47. R. Jackstadt *et al.*, Epithelial NOTCH Signaling Rewires the Tumor Microenvironment of Colorectal Cancer to Drive Poor-Prognosis Subtypes and Metastasis. *Cancer Cell* **36**, 319-336 e317 (2019).
48. S. Go *et al.*, Tissue-resident NK cells support survival in pancreatic cancer through promotion 1 of cDC1-CD8T activity. *bioRxiv* **https://doi.org/10.1101/2023.10.14.56233**, (2023).
49. J. E. East *et al.*, British Society of Gastroenterology position statement on serrated polyps in the colon and rectum. *Gut* **66**, 1181-1196 (2017).
50. A. Junca *et al.*, Detection of Colorectal Cancer and Advanced Adenoma by Liquid Biopsy (Decalib Study): The ddPCR Challenge. *Cancers (Basel)* **12**, (2020).

51. M. Galanopoulos *et al.*, Comparative Study of Mutations in Single Nucleotide Polymorphism Loci of KRAS and BRAF Genes in Patients Who Underwent Screening Colonoscopy, With and Without Premalignant Intestinal Polyps. *Anticancer Res* **37**, 651-657 (2017).
52. M. G. Best, P. Wesseling, T. Wurdinger, Tumor-Educated Platelets as a Noninvasive Biomarker Source for Cancer Detection and Progression Monitoring. *Cancer Res* **78**, 3407-3412 (2018).
53. S. A. Joosse, K. Pantel, Tumor-Educated Platelets as Liquid Biopsy in Cancer Patients. *Cancer Cell* **28**, 552-554 (2015).
54. D. C. Calverley *et al.*, Significant downregulation of platelet gene expression in metastatic lung cancer. *Clin Transl Sci* **3**, 227-232 (2010).
55. G. H. Frydman *et al.*, Megakaryocytes contain extranuclear histones and may be a source of platelet-associated histones during sepsis. *Sci Rep* **10**, 4621 (2020).
56. L. Clejan, H. Menahem, Binding of deoxyribonucleic acid to the surface of human platelets. *Acta Haematol* **58**, 84-88 (1977).
57. C. A. Dorsch, Binding of single-strand DNA to human platelets. *Thromb Res* **24**, 119-129 (1981).
58. C. Vanpouille-Box, S. Demaria, S. C. Formenti, L. Galluzzi, Cytosolic DNA Sensing in Organismal Tumor Control. *Cancer Cell* **34**, 361-378 (2018).
59. Y. Wang *et al.*, eccDNAs are apoptotic products with high innate immunostimulatory activity. *Nature* **599**, 308-314 (2021).
60. I. Hawwari *et al.*, Platelet-derived transcription factors licence human monocyte inflammation. *bioRxiv*, (2023).
61. E. S. Kim *et al.*, Blood-based tumor mutational burden as a biomarker for atezolizumab in non-small cell lung cancer: the phase 2 B-F1RST trial. *Nat Med* **28**, 939-945 (2022).
62. D. G. Rothwell *et al.*, Utility of ctDNA to support patient selection for early phase clinical trials: the TARGET study. *Nat Med* **25**, 738-743 (2019).
63. J. D. Merker *et al.*, Circulating Tumor DNA Analysis in Patients With Cancer: American Society of Clinical Oncology and College of American Pathologists Joint Review. *J Clin Oncol* **36**, 1631-1641 (2018).
64. N. Liang *et al.*, Mature Red Blood Cells Contain Long DNA Fragments and Could Acquire DNA from Lung Cancer Tissue. *Adv Sci (Weinh)* **10**, e2206361 (2023).
65. C. Schmidl, A. F. Rendeiro, N. C. Sheffield, C. Bock, ChIPmentation: fast, robust, low-input ChIP-seq for histones and transcription factors. *Nature Methods* **12**, 963-965 (2015).
66. J. D. Buenrostro, B. Wu, H. Y. Chang, W. J. Greenleaf, ATAC-seq: A Method for Assaying Chromatin Accessibility Genome-Wide. *Curr Protoc Mol Biol* **109**, 21.29.21-21.29.29 (2015).
67. Y. Jung, L. Wen, A. Altman, K. Ley, CD45 pre-exclusion from the tips of T cell microvilli prior to antigen recognition. *Nat Commun* **12**, 3872 (2021).
68. S. Andrews. (Babraham Bioinformatics, Babraham Institute, Cambridge, United Kingdom, 2010).
69. F. Krueger, F. James, P. Ewels, E. Afyounian, B. Schuster-Boeckler, FelixKrueger/TrimGalore: v0. 6.7-DOI via Zenodo. *Zenodo https://zenodo. org/record/5127899 (Accessed February 23, 2022)*, (2021).

70. V. A. Schneider *et al.*, Evaluation of GRCh38 and de novo haploid genome assemblies demonstrates the enduring quality of the reference assembly. *Genome Res* **27**, 849-864 (2017).
71. H. Li, Aligning sequence reads, clone sequences and assembly contigs with BWA-MEM. *arXiv preprint arXiv:1303.3997*, (2013).
72. H. Li *et al.*, The Sequence Alignment/Map format and SAMtools. *Bioinformatics* **25**, 2078-2079 (2009).
73. G. Van der Auwera, B. O'Connor, Safari, an OMC Using Docker, GATK, and WDL in Terra. *Genomics in the Cloud* **300**, (2020).
74. H. M. Amemiya, A. Kundaje, A. P. Boyle, The ENCODE Blacklist: Identification of Problematic Regions of the Genome. *Sci Rep* **9**, 9354 (2019).
75. A. R. Quinlan, I. M. Hall, BEDTools: a flexible suite of utilities for comparing genomic features. *Bioinformatics* **26**, 841-842 (2010).
76. H. Wickham, in *ggplot2*. (Springer, 2016), pp. 189-201.
77. I. Abugessaisa *et al.*, refTSS: a reference data set for human and mouse transcription start sites. *Journal of molecular biology* **431**, 2407-2422 (2019).
78. M. Karimzadeh, C. Ernst, A. Kundaje, M. M. Hoffman, Umap and Bismap: quantifying genome and methylome mappability. *Nucleic acids research* **46**, e120-e120 (2018).
79. B. Gel, E. Serra, karyoploteR: an R/Bioconductor package to plot customizable genomes displaying arbitrary data. *Bioinformatics* **33**, 3088-3090 (2017).
80. C. Gini, On the measure of concentration with special reference to income and statistics. *Colorado College Publication, General Series* **208**, 73-79 (1936).
81. P. Siejka-Zielińska *et al.*, Cell-free DNA TAPS provides multimodal information for early cancer detection. *Sci Adv* **7**, eabh0534 (2021).
82. B. Schuster-Boeckler, & Inchauspe, J., Scripts and Outputs for Murphy et al. *Zenodo*, (2022).

Acknowledgments:
We thank Jana Koth and Christoffer Lagerholm from the MRC WIMM Imaging Facility, Henkjan Gersen, Kennith Meissner, Fenella Roseman, Jill Brown, Nawshad Hayder, Mick Jacobs and Daniela Moralli for ideas and support with experiments, the COMBATcancer consortium and the CRUK Oxford Centre. We thank the patients and healthy donors for their participation in the research, and the Oxford COMBATcancer Consortium and CRUK Oxford Centre for helping with recruitment and sample banking. We also acknowledge BioRender for figure creation.

Funding:
Cancer Research UK Early Detection Project Grant EDDCPJT/1000003 (BP, CDG, PR); CRUK Advanced Clinical Scientist Fellowship C67633/A29034 (BP); Senior Fellowship RCCSCF-May24/100001 funded by Cancer Research UK in partnership with the Rosetrees Trust (BP); Ludwig Institute for Cancer Research Associate Member Program (BP, BSB); Medical Research Council Grant MR/T04490X/1 (BSB); Kidani Memorial Trust (EON); CRUK Oxford Centre Clinical Research Training Fellowship C130623/A249471 (NS) and an unrestricted research grant from Emerson Health (now Yosemite) (BP). We would also like to acknowledge support from the National Institute for Health Research (NIHR), Oxford Biomedical Research Centre (BRC) and CRUK Oxford Centre Grant CTRQQR-2021\100002.

Author contributions:
Conceptualization: LM, BP, CDG. Methodology: LM, JI, NS, HLBD, PH, GV, RL, NJJ, CB, EM, ZE, LC, ES, LD, SK, IH, MK, EON, MV, PR, SL, BSB, CDG, BP. Software: JI, BSB, JRH. Validation: LM, JI, PR, CDG, BP, BSB, CB, NJJ. Formal analysis: LM, JI, BSB, PR. Investigation: LM, JI, NS, HLBD, PH, GV, RL, NJJ, CB, SB, ZE, LC, JOS, MPR, AOK, CSK, NN, EM, ES, LD. Resources: LM, NS, BSB, CDG, PR, SL, MD, MV, EON, NN. Data curation: LM, JI, BSB, JRH, ZE, SB, LC, PR. Writing - original draft: LM, BP. Writing - review & editing: all authors Visualization: LM, JI, ZE, LC, BSB. Supervision: BP, AJM, PR, CDG, BSB, JRH. Project administration: LM, BP, CDG, BSB. Funding acquisition: BP, CDG, BSB.

Competing interests:
BP, AJM, CGC, LM, and NS are listed as inventors on patent GB2203947.3 (CRUK Ref: CR/2021-069), submitted in 2022 by the University of Oxford, which covers the detection of disease-associated gene mutations in nucleic acids derived from purified platelets. BP, AJM, and LM are also inventors on patent P45651WO1 (GB2314848.9), filed in 2023 by the University of Oxford, relating to the recovery of cell-free nucleic acids from platelets. BP is a co-founder and major shareholder of Alethiomics, has received honoraria for speaking engagements and/or advisory work for Incyte, BMS, Constellation Therapeutics, GSK, Blueprint Medicines, Novartis and Alethiomics and received research funding from Incyte, Galecto and Alethiomics. AJM is a co-founder and shareholder of Alethiomics, has received honoraria/served on advisory boards for Alethiomics, Novartis, CTI, Gilead and Shire has received research funding from Alethiomics and Galecto. LM has consulted for Alethiomics. All other authors declare that they have no conflicts of interest.

Data and materials availability:

All data needed to evaluate the conclusions in the paper are present in the paper or the Supplementary Materials. Raw whole genome sequencing data has been deposited in the European Genome-phenome Archive (EGA) under accession number EGAS00001006854 (Study: EGA00001006854; Dataset EGAD00001009856; Data Access Committee: EGAC00001003034). Code is available from Zenodo (*82*).

Supplementary Materials List:

Supplementary Text
Figs. S1 to S6
Tables S1 to S7
Supplementary Movies S1 to S6

MDAR Reproducibility Checklist

Figure 1

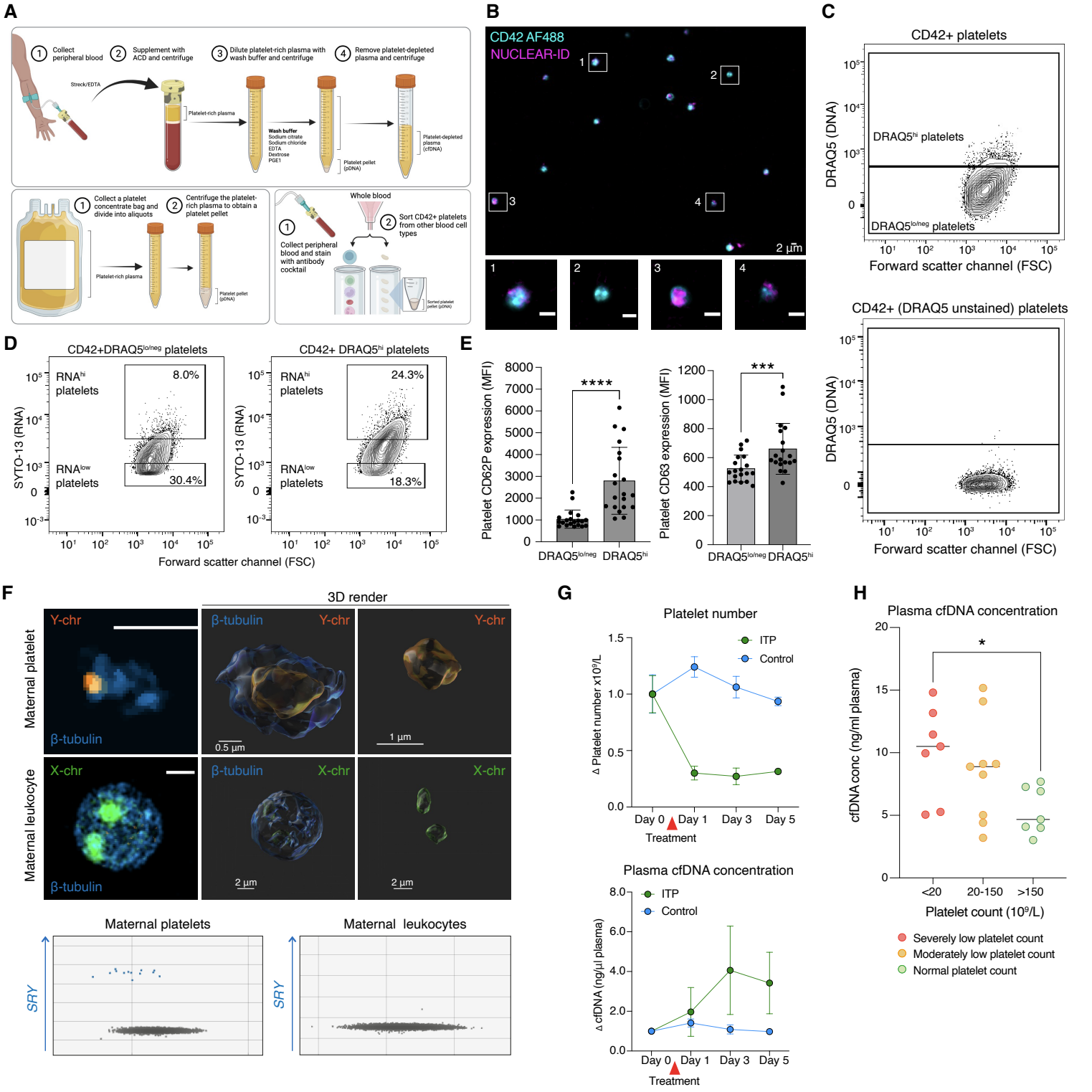

A
Collect peripheral blood
Supplement with ACD and centrifuge
Dilute platelet-rich plasma with wash buffer and centrifuge
Remove platelet-depleted plasma and centrifuge
Streck/EDTA
Platelet-rich plasma
Wash buffer
Sodium citrate
Sodium chloride
EDTA
Dextrose
PGE1
Platelet pellet (pDNA)
Platelet-depleted plasma (cfDNA)
Collect a platelet concentrate bag and divide into aliquots
Centrifuge the platelet-rich plasma to obtain a platelet pellet
Whole blood
Collect peripheral blood and stain with antibody cocktail
Sort CD42+ platelets from other blood cell types
B
CD42 AF488
NUCLEAR-ID
2 µm
C
CD42+ platelets
DRAQ5hi platelets
DRAQ5lo/neg platelets
DRAQ5 (DNA)
Forward scatter channel (FSC)
CD42+ (DRAQ5 unstained) platelets
D
CD42+DRAQ5lo/neg platelets
CD42+ DRAQ5hi platelets
RNAhi platelets
RNAlow platelets
8.0%
30.4%
24.3%
18.3%
SYTO-13 (RNA)
Forward scatter channel (FSC)
E
Platelet CD62P expression (MFI)
Platelet CD63 expression (MFI)
****
***
DRAQ5lo/neg
DRAQ5hi
F
3D render
Maternal platelet
Maternal leukocyte
Y-chr
X-chr
β-tubulin
0.5 µm
1 µm
2 µm
Maternal platelets
Maternal leukocytes
SRY
G
Platelet number
ITP
Control
Δ Platelet number x10⁹/L
Day 0
Day 1
Day 3
Day 5
Treatment
Plasma cfDNA concentration
Δ cfDNA (ng/µl plasma)
H
Plasma cfDNA concentration
cfDNA conc (ng/ml plasma)
*
<20
20-150
>150
Platelet count (10⁹/L)
Severely low platelet count
Moderately low platelet count
Normal platelet count

Fig. 1. Platelets sequester DNA during circulation. (A) Schematic showing sources of purified platelets. Top, sequential centrifugation of peripheral blood to simultaneously extract DNA from a platelet pellet (pDNA) and platelet-depleted plasma (cfDNA); bottom left, centrifugation of healthy donor plateletpheresis concentrates to obtain a platelet pellet; bottom right, fluorescence-activated cell sorting of whole blood. **(B)** Healthy donor-derived platelets identified by CD42 AF488 (cyan) show an internal fluorescent signal for NUCLEAR-ID, a cell permeable dye that intercalates with double stranded DNA (magenta). White boxes show magnified regions, representative images shown, scale bars represent 2 μm. **(C)** Flow cytometric analysis of CD42+ healthy donor-derived platelets stained with and without the DNA marker DRAQ5. Top, 8% of circulating platelets stain strongly positive for DRAQ5, *n* = 20 healthy donors concatenated into a single FCS file. Bottom, single CD42+ stained platelets show no DRAQ5 autofluorescence, *n* = 10 healthy donors, concatenated data shown. **(D)** Flow cytometric analysis quantifying RNA content (SYTO-13 positivity) of CD42+, DRAQ5-hi and DRAQ5-lo/neg platelets (*n* = 10 healthy donors, concatenated data shown). **(E)** Platelets with a higher DNA content (DRAQ5-hi) showed higher levels of activation as determined by P-selectin (CD62P) and CD63 expression. Each dot represents an individual healthy donor. *n* = 19-20 donors for CD63 and CD62P, respectively. Bars show mean ± SD, ***$P < 0.001$; ****$P < 0.0001$; as determined by a Wilcoxon signed-rank test. **(F)** FISH and ddPCR showing detection of the Y-chromosome gene *SRY* in maternal platelets, but not leukocytes sampled from mothers of male offspring prior to delivery. Platelets and leukocytes were counterstained with β-tubulin (blue) and imaged using a ZEISS LSM900, 63X magnification. Representative images and ddPCR data shown, 3D rendering performed using ImarisViewer. *n* = 5 female donors (FISH) and *n* = 25 female donors (ddPCR). **(G)** Rise in cfDNA following acute depletion of platelets in healthy mice following administration of an anti-platelet antibody. *n* = 5 mice per day, *n* = 20 mice per condition. Each dot shows mean ± SEM fold change at Day 1, 3 and 5 compared to baseline (Day 0, untreated mice). **(H)** Plasma cfDNA concentrations (ng/ml) for patients with ITP and severely (< 20 $x10^9$/L, *n* = 7) or moderately (20 - 150 $x10^9$/L, *n* = 9) low platelet counts or counts in the normal range ($\geq$ 150 $x10^9$/L, *n* = 7), *$P < 0.05$; for a Mann- Whitney *U* test, each point shows data from one individual, with line at the median. ddPCR, droplet digital PCR; FISH, fluorescence *in situ* hybridization; ITP, immune thrombocytopenic purpura; MFI, mean fluorescence intensity; *SRY*, sex-determining region Y.

Figure 2

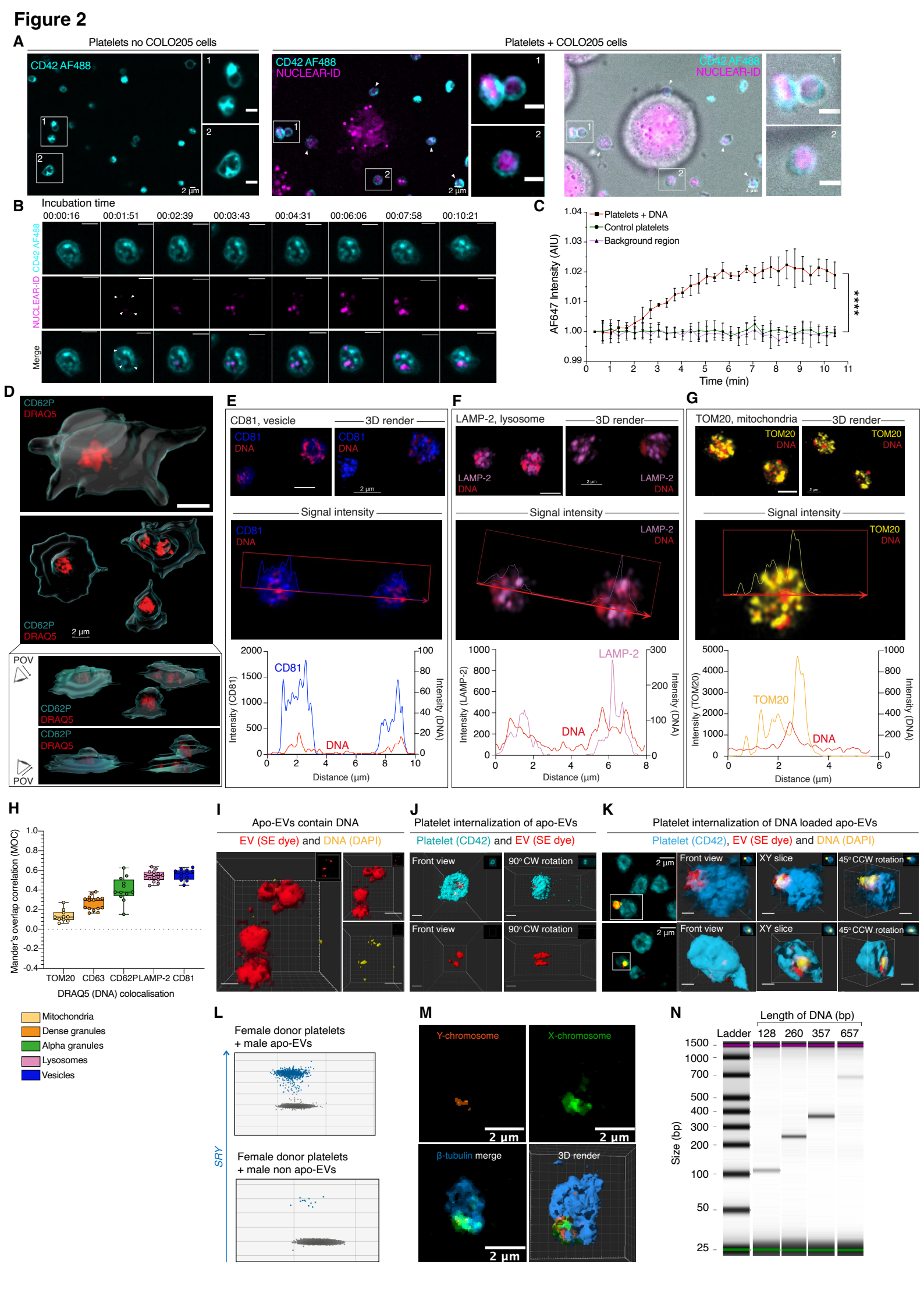

A
Platelets no COLO205 cells
Platelets + COLO205 cells
CD42 AF488
NUCLEAR-ID
2 µm
B
Incubation time
00:00:16
00:01:51
00:02:39
00:03:43
00:04:31
00:06:06
00:07:58
00:10:21
CD42 AF488
NUCLEAR-ID
Merge
C
Platelets + DNA
Control platelets
Background region
AF647 Intensity (AIU)
Time (min)
****
D
CD62P
DRAQ5
POV
E
CD81, vesicle
3D render
CD81
DNA
Signal intensity
Intensity (CD81)
Intensity (DNA)
Distance (µm)
F
LAMP-2, lysosome
LAMP-2
G
TOM20, mitochondria
TOM20
H
Mander's overlap correlation (MOC)
TOM20
CD63
CD62P
LAMP-2
CD81
DRAQ5 (DNA) colocalisation
Mitochondria
Dense granules
Alpha granules
Lysosomes
Vesicles
I
Apo-EVs contain DNA
EV (SE dye) and DNA (DAPI)
J
Platelet internalization of apo-EVs
Platelet (CD42) and EV (SE dye)
Front view
90° CW rotation
K
Platelet internalization of DNA loaded apo-EVs
Platelet (CD42), EV (SE dye) and DNA (DAPI)
XY slice
45° CCW rotation
L
Female donor platelets
+ male apo-EVs
Female donor platelets
+ male non apo-EVs
SRY
M
Y-chromosome
X-chromosome
β-tubulin merge
3D render
N
Length of DNA (bp)
Ladder
128
260
357
657
Size (bp)

Fig. 2. Platelets rapidly internalize DNA released by nucleated cells via uptake of DNA-loaded extracellular vesicles (EVs) and non-membrane encapsulated DNA fragments. (A) Healthy donor-derived, CD42 AF488 (cyan)-labeled platelets before (left) and after (middle and right) co-incubation with COLO205 cells labeled with NUCLEAR-ID (magenta) to track DNA transfer. White boxes show magnified regions; arrows highlight platelet uptake of COLO25-derived DNA and scale bars represent 2 µm. Middle (fluorescence) and far right (brightfield) are the same image. **(B)** Live-cell time-lapse imaging of a representative platelet showing internalization of DNA. Scale bars represent 3 µm. **(C)** Time-course quantification of platelet DNA fluorescence intensity, data points show mean ± SD. AF647 signal was measured in background regions to detect fluctuations. ****$P < 0.0001$; as determined by a Wilcoxon signed-rank test. Tracking shown for platelets incubated with control media ($n = 168$ platelets) or media conditioned by NUCLEAR-ID-labeled COLO205 cells ($n = 173$ platelets). **(D-G)** Representative images acquired using the Airyscan detector of a ZEISS LSM980 and 3D rendering performed using ImarisViewer. **(D)** Healthy donor platelets spread on collagen, stained with CD62P to create a translucent cell surface mask (turquoise) and DRAQ5 (DNA, red). Four representative platelets shown. Bottom panel shows alternate views of the same platelets from above and below, scale bars represent 2 µm. **(E-G)** Top, representative images and 3D renders of two healthy donor platelets showing co-localization of platelet DNA (DRAQ5, red) with **(E)** CD81 (vesicles, blue), **(F)** LAMP-2 (lysosomes, pink), and **(G)** TOM20 (mitochondria, yellow). Bottom, pixel intensity (y-axis) along defined lines (distance in µm, x-axis) was analyzed using ZEISS Zen software. **(H)** Manders' correlation coefficients were calculated for DNA with mitochondria (TOM20), dense granules (CD63), alpha granules (CD62P), lysosomes (LAMP-2), and vesicles (CD81). Box plots show the median, Q1, and Q3, with whiskers extending to minimum and maximum values. Platelets analyzed per marker: TOM20 ($n = 10$), CD63 ($n = 15$), CD62P ($n = 12$), LAMP-2 ($n = 15$), and CD81 ($n = 12$). **(I)** A representative 3D reconstruction of EV clusters released by apoptotic BL2 cells labeled with an amine-reactive membrane dye (CF658, red) and DNA stain (DAPI, yellow), revealing internalized DNA. Imaged using a ZEISS LSM900, 63X magnification. Scale bars represent 2 µm. **(J)** Platelets stained with CD42 AF488 (cyan) following incubation with labeled EVs (red), showing three EVs within a single representative platelet. 3D modeling shows 90° clockwise rotation. Scale bar represents 1.4 µm. **(K)** 3D reconstruction showing platelet internalization of DNA-loaded apo-EVs (DNA: yellow, EVs: red). Two representative platelets are shown: one with surface-bound DNA-loaded EVs (top) and one with internalized EVs (bottom). Scale bars represent 0.5 µm unless stated otherwise. **(L)** ddPCR quantification of the Y-chromosome gene *SRY* in DNA derived from platelets of a female donor after incubation with apo-EVs and non-apo EVs. Representative data from $n = 3$ independent experiments. **(M)** Representative FISH and 3D render demonstrating fragments of X- and Y- chromosomes in female donor platelets following incubation with male HEL cells. Platelets counterstained with β-tubulin (blue). Imaged using a ZEISS LSM900, 63X magnification and 3D render created using ImarisViewer. **(N)** Electrophoresis data showing recovery of 128-657 bp synthetic DNA fragments from washed healthy donor platelets after overnight incubation. Representative data from $n = 5$ independent experiments. AIU, arbitrary intensity units; apo, apoptotic; BL2, Burkitt's lymphoma cells; chr, chromosome; CCW, counterclockwise; CW, clockwise; EVs, extracellular vesicles; FISH, fluorescence *in situ* hybridization; POV, perspective of view; SE, succinimidyl ester; *SRY*, sex-determining region Y.

Figure 3

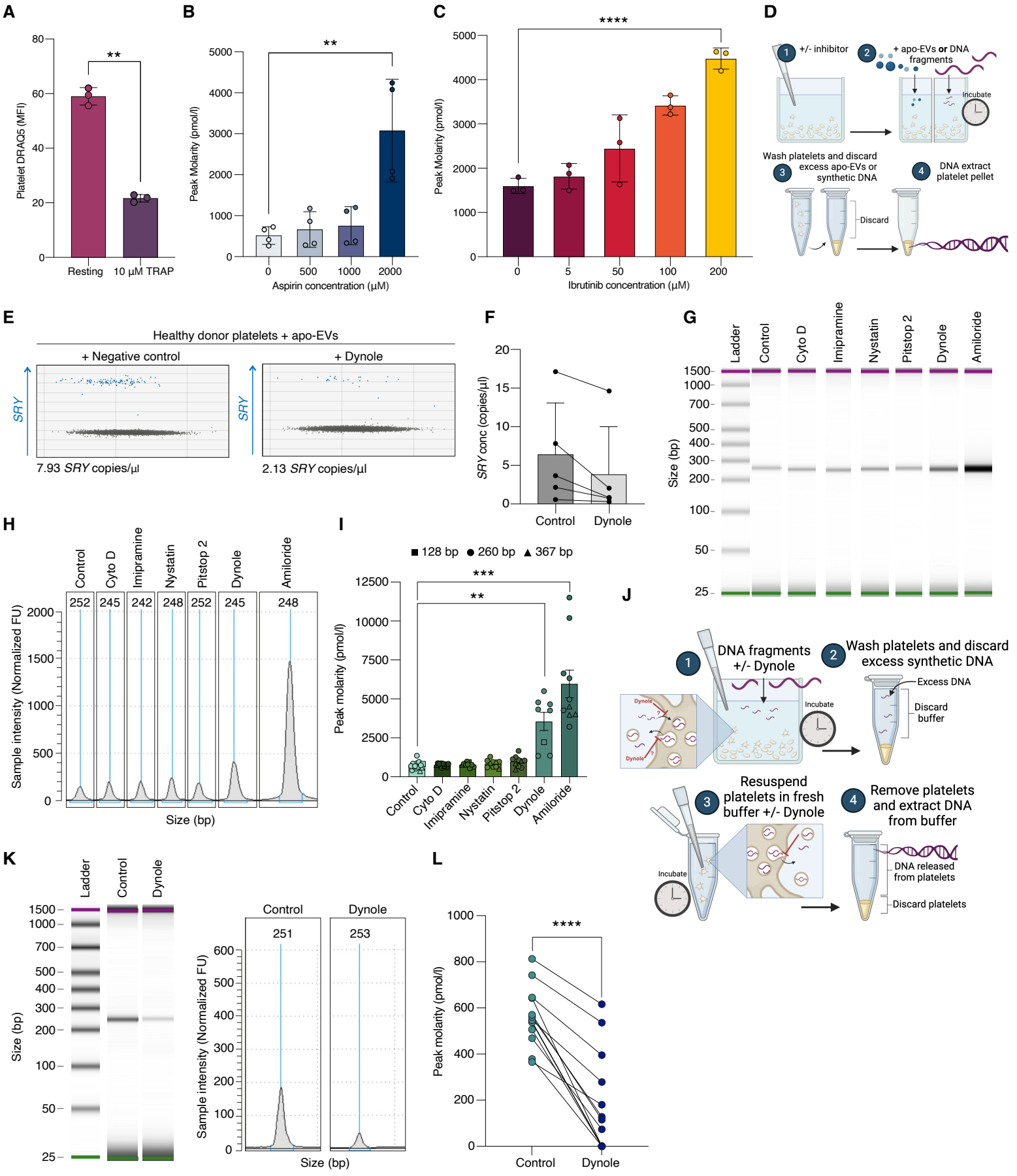

A
Platelet DRAQ5 (MFI)
Resting
10 µM TRAP
B
Peak Molarity (pmol/l)
Aspirin concentration (µM)
C
Peak Molarity (pmol/l)
Ibrutinib concentration (µM)
D
+/- inhibitor
+ apo-EVs or DNA fragments
Incubate
Wash platelets and discard excess apo-EVs or synthetic DNA
DNA extract platelet pellet
Discard
E
Healthy donor platelets + apo-EVs
+ Negative control
+ Dynole
SRY
7.93 SRY copies/µl
2.13 SRY copies/µl
F
SRY conc (copies/µl)
Control
Dynole
G
Ladder
Control
Cyto D
Imipramine
Nystatin
Pitstop 2
Dynole
Amiloride
Size (bp)
H
Control
Cyto D
Imipramine
Nystatin
Pitstop 2
Dynole
Amiloride
252
245
242
248
252
245
248
Sample intensity (Normalized FU)
Size (bp)
I
128 bp
260 bp
367 bp
Peak molarity (pmol/l)
J
DNA fragments +/- Dynole
Wash platelets and discard excess synthetic DNA
Excess DNA
Discard buffer
Incubate
Resuspend platelets in fresh buffer +/- Dynole
Remove platelets and extract DNA from buffer
DNA released from platelets
Discard platelets
K
Ladder
Control
Dynole
Size (bp)
Control
Dynole
251
253
Sample intensity (Normalized FU)
Size (bp)
L
Peak molarity (pmol/l)
Control
Dynole

Fig. 3. Platelet DNA content can be pharmacologically modulated. (A) Flow cytometric analysis of DNA (DRAQ5) content in healthy donor-derived platelets, with and without activation using 10 μM TRAP-6. *n* = 3, points represent data from individual healthy donors, bars show mean ± SD, ***P* < 0.01; as determined by a paired *t* test. **(B, C)** Inhibition of platelet activation with **(B)** aspirin or **(C)** ibrutinib increases the yield of DNA from platelet pellets. *n* = 3-4 independent experiments, plots show mean ± SD peak molarity corresponding to DNA TapeStation peaks for synthetic DNA fragments co-incubated with platelets prior to washing and DNA extraction. ***P* < 0.01; *****P* < 0.0001; as determined by an unpaired *t* test. **(D)** Schematic of the method for investigating DNA uptake. Platelets were pre-treated with inhibitors, incubated with DNA-loaded apoptotic BL2-derived EVs (apo-EVs) or synthetic DNA fragments, then washed, pelleted, and subjected to DNA extraction. **(E, F)** ddPCR quantification of *SRY* in platelet-derived DNA from female donors after incubation of platelets with apo-EVs treated with or without Dynole. Fewer *SRY* copies were detected in dynamin-inhibited platelets compared to controls. **(E)** Representative ddPCR plot and **(F)** *n* = 5 independent experiments, paired line plot shows mean ± SD, with lines connecting data points before and after inhibition. **(G, H)** Representative electrophoresis showing recovery of 260 bp synthetic DNA fragments from platelets treated with inhibitors known to block components of cargo trafficking. More DNA was extracted from platelets treated with Dynole and amiloride. **(I)** Summary plot showing mean ± SD for all DNA fragment lengths (128-367 bp) following treatment with inhibitors (G, H). Data from four independent experiments (*n* = 4), with 2-5 replicate wells per condition. ***P* < 0.01; ****P* < 0.001; as determined by a paired *t* test. **(J)** Schematic of the method for investigating platelet DNA release. Platelets were treated with or without Dynole, incubated with synthetic DNA, washed, resuspended in fresh buffer, and incubated for 3 hours. DNA was then extracted from platelet-depleted buffer. **(K)** Representative electrophoresis and **(L)** a paired-line plot showing significant inhibition of platelet DNA release following Dynole treatment, with lines connecting data points before and after inhibition. Data from five independent experiments (*n* = 5), with 2-3 replicate wells per condition. *****P* < 0.0001; as determined by a paired *t* test. Apo, apoptotic; cyto D, cytochalasin D; ddPCR, droplet digital PCR; EVs, extracellular vesicles; FU, fluorescence units. *SRY*, sex-determining region Y.

Figure 4

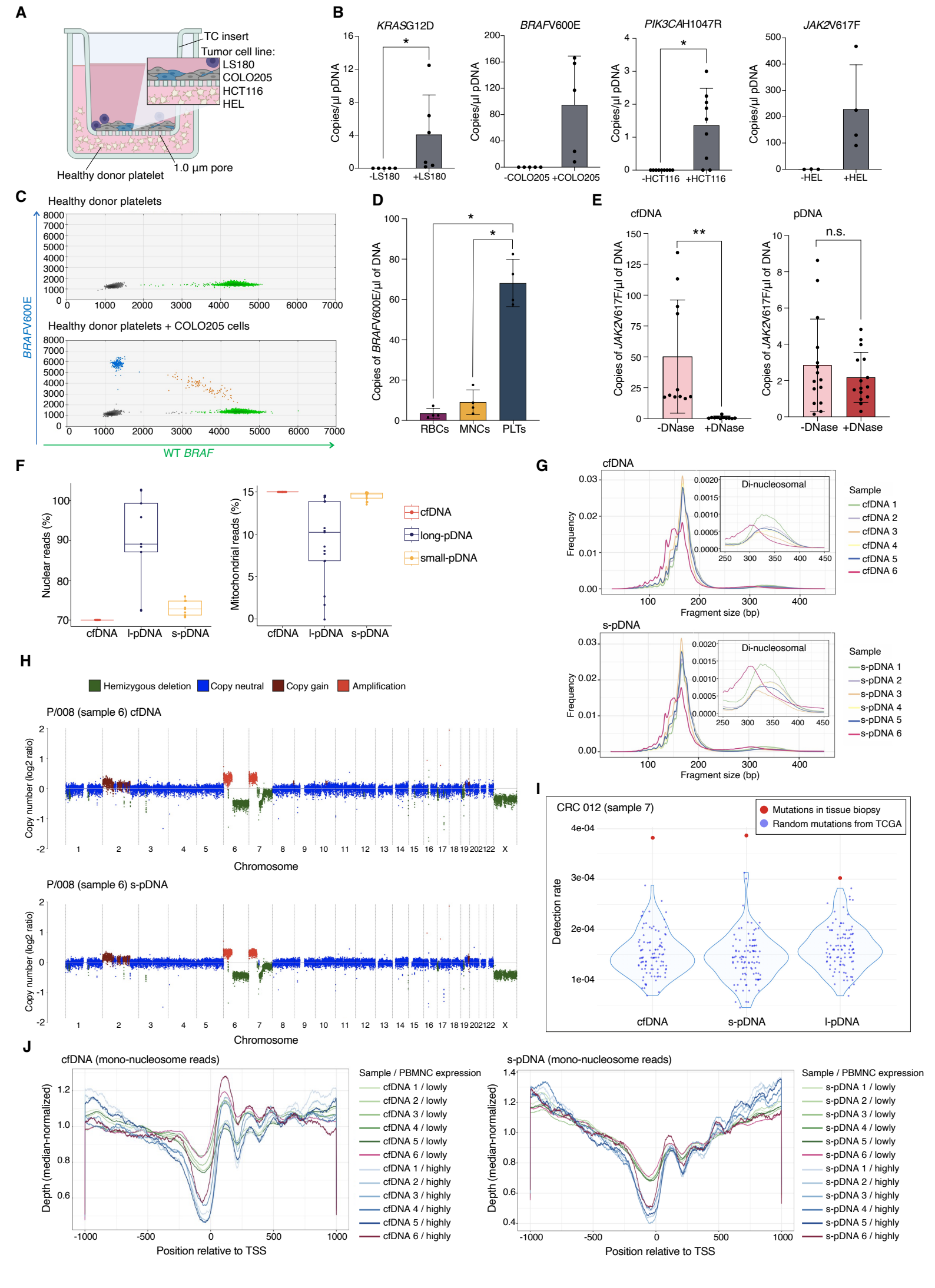

A
TC insert
Tumor cell line:
LS180
COLO205
HCT116
HEL
Healthy donor platelet
1.0 µm pore
B
KRASG12D
BRAFV600E
PIK3CAH1047R
JAK2V617F
Copies/µl pDNA
-LS180 +LS180
-COLO205 +COLO205
-HCT116 +HCT116
-HEL +HEL
C
Healthy donor platelets
Healthy donor platelets + COLO205 cells
BRAFV600E
WT BRAF
D
Copies of BRAFV600E/µl of DNA
RBCs MNCs PLTs
E
cfDNA
pDNA
Copies of JAK2V617F/µl of DNA
-DNase +DNase
n.s.
F
Nuclear reads (%)
Mitochondrial reads (%)
cfDNA l-pDNA s-pDNA
cfDNA
long-pDNA
small-pDNA
G
cfDNA
s-pDNA
Frequency
Fragment size (bp)
Di-nucleosomal
Sample
cfDNA 1
cfDNA 2
cfDNA 3
cfDNA 4
cfDNA 5
cfDNA 6
s-pDNA 1
s-pDNA 2
s-pDNA 3
s-pDNA 4
s-pDNA 5
s-pDNA 6
H
Hemizygous deletion
Copy neutral
Copy gain
Amplification
P/008 (sample 6) cfDNA
P/008 (sample 6) s-pDNA
Copy number (log2 ratio)
Chromosome
I
CRC 012 (sample 7)
Mutations in tissue biopsy
Random mutations from TCGA
Detection rate
cfDNA s-pDNA l-pDNA
J
cfDNA (mono-nucleosome reads)
s-pDNA (mono-nucleosome reads)
Depth (median-normalized)
Position relative to TSS
Sample / PBMNC expression
cfDNA 1 / lowly
cfDNA 2 / lowly
cfDNA 3 / lowly
cfDNA 4 / lowly
cfDNA 5 / lowly
cfDNA 6 / lowly
cfDNA 1 / highly
cfDNA 2 / highly
cfDNA 3 / highly
cfDNA 4 / highly
cfDNA 5 / highly
cfDNA 6 / highly
s-pDNA 1 / lowly
s-pDNA 2 / lowly
s-pDNA 3 / lowly
s-pDNA 4 / lowly
s-pDNA 5 / lowly
s-pDNA 6 / lowly
s-pDNA 1 / highly
s-pDNA 2 / highly
s-pDNA 3 / highly
s-pDNA 4 / highly
s-pDNA 5 / highly
s-pDNA 6 / highly

Fig. 4. Platelets contain a repertoire of DNA fragments that map over the human nuclear genome, including tumor-derived DNA bearing cancer-associated gene mutations. (A) Schematic of the experimental system for co-incubating healthy donor platelets with malignant cells, separated by 1 μm membrane inserts to allow extracellular biomolecule and small EV exchange while preventing cell transfer. After co-incubation, platelets were removed, washed three times, and subjected to DNA extraction. **(B)** Number of copies of mutant alleles detected per μl of DNA extracted from platelets incubated with (+) or without (-) colorectal (LS180, COLO205 and HCT116) and erythroleukemia (HEL) cell lines. Data were collected from one to three independent experiments, with 3-5 replicate wells per condition. Each point represents one co-culture experiment per condition. Replicates per condition were as follows: LS180 (*n* = 2 experiments; 3 replicates each), COLO205 (*n* = 1 experiment; 4 and 5 replicates), HCT116 (*n* = 3 experiments; 3 replicates each), and HEL (*n* = 1 experiment; 3 and 4 replicates). Bars represent mean ± SD, **P* < 0.05; as determined by a Wilcoxon paired signed rank test. **(C)** Representative ddPCR analysis showing quantification of wild-type *BRAF* and *BRAF*V600E alleles in pDNA extracted from healthy donor platelets before (top) and after co-incubation with COLO205 colorectal cancer cells (bottom). **(D)** Quantification of *BRAF*V600E in red blood cells, mononuclear cells and platelets following incubation in media conditioned by COLO205 cells. Data are presented as mean ± SD*, n* = 2, individual points represent independent experiments, each with 2 replicates. **P* < 0.05; as determined by a Mann- Whitney *U* test. **(E)** Impact of DNase treatment on the detection of *JAK2* mutant alleles in pDNA and cfDNA (media) following co-incubation of healthy donor platelets with HEL cells. Data are presented as mean ± SD, *n* = 5, points represent independent experiments, each with 3 replicates. n.s., not significant; ***P* < 0.01; determined by a Wilcoxon signed-rank test. **(F)** Percentage of fragments mapping to the nuclear and mitochondrial genomes from cell free DNA, short (> 100 and < 600 bp) and long (> 600 bp) platelet DNA fragments. In the box plot, the center line shows the median, whiskers indicate the minimum and maximum values, and each data point represents one patient, *n* = 15 donors with gastrointestinal carcinoma. **(G)** Fragment length distribution of paired, aligned reads for cfDNA (top) and s-pDNA (bottom). *n* = 6 donors with gastrointestinal carcinoma, samples 1-5 show a primary peak at ~165 bp (mono-nucleosomal) and a smaller secondary peak at ~325 bp (di-nucleosomal, inset). Sample 6 (red line), from a patient with untreated pancreatic adenocarcinoma, has shorter mono- and di-nucleosomal fragments than samples 1-5 (post anti-cancer therapy patients). **(H)** Deviation from median coverage in 100 kbp windows across all chromosomes for cfDNA (top) and s-pDNA (bottom) for P/008 (sample 6), revealing chromosomal aberrations in chromosomes 2, 6 and 7 (copy number gains and amplifications shown in red, deletions in green). **(I)** Detection rates of mutations in cfDNA, s-pDNA and l-pDNA for sample 7 where matched tumor biopsy was available. The red dot indicates mutations detected in the tumor biopsy; blue dots indicate 100 random samples of mutations from other patients with colorectal carcinoma from The Cancer Genome Atlas dataset. **(J)** Read depth distribution around transcription start sites of genes highly (TPM >15, blue) and lowly (TPM <15, green) expressed in peripheral blood mononuclear cells for cfDNA (left) and s-pDNA (right) mononucleosome reads. *n* = 6 donors with gastrointestinal carcinoma, depth per position per sample was normalized to the median read depth across all genes in that expression category. MNC, mononuclear cells; PLTs, platelets; RBC, red blood cells; TCGA, The Cancer Genome Atlas; TPM, transcripts per million; TSS, transcriptional start site; WT, wild type.

Figure 5

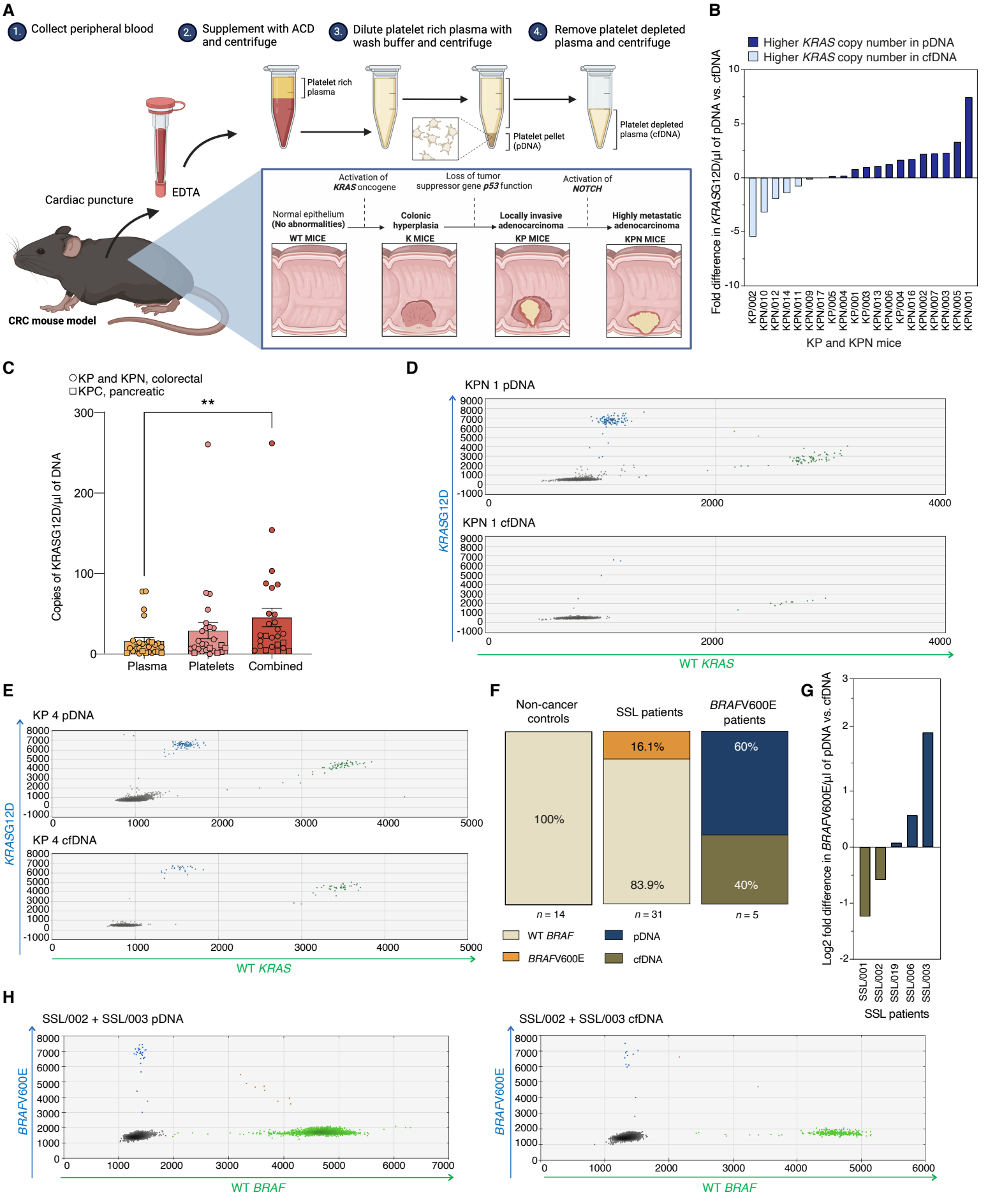

A
1. Collect peripheral blood
2. Supplement with ACD and centrifuge
3. Dilute platelet rich plasma with wash buffer and centrifuge
4. Remove platelet depleted plasma and centrifuge
Platelet rich plasma
Platelet pellet (pDNA)
Platelet depleted plasma (cfDNA)
EDTA
Cardiac puncture
CRC mouse model
Activation of KRAS oncogene
Loss of tumor suppressor gene p53 function
Activation of NOTCH
Normal epithelium (No abnormalities)
Colonic hyperplasia
Locally invasive adenocarcinoma
Highly metastatic adenocarcinoma
WT MICE
K MICE
KP MICE
KPN MICE
B
Higher KRAS copy number in pDNA
Higher KRAS copy number in cfDNA
Fold difference in KRASG12D/µl of pDNA vs. cfDNA
KP and KPN mice
C
KP and KPN, colorectal
KPC, pancreatic
Copies of KRASG12D/µl of DNA
Plasma
Platelets
Combined
D
KPN 1 pDNA
KPN 1 cfDNA
KRASG12D
WT KRAS
E
KP 4 pDNA
KP 4 cfDNA
KRASG12D
WT KRAS
F
Non-cancer controls
SSL patients
BRAFV600E patients
100%
16.1%
83.9%
60%
40%
n = 14
n = 31
n = 5
WT BRAF
BRAFV600E
pDNA
cfDNA
G
Log2 fold difference in BRAFV600E/µl of pDNA vs. cfDNA
SSL/001
SSL/002
SSL/019
SSL/006
SSL/003
SSL patients
H
SSL/002 + SSL/003 pDNA
SSL/002 + SSL/003 cfDNA
BRAFV600E
WT BRAF

Fig. 5. Detection of driver mutations in pDNA and cfDNA from mice with localized and metastatic colorectal adenocarcinoma, and patients with pre-malignant colonic lesions. **(A)** Schematic showing isolation of platelet DNA (pDNA) and cell free (cfDNA) from C57BL/6 mice expressing *KRAS*G12D and *TP53* (KP) mutations via the villin promotor resulting in locally invasive colorectal adenocarcinoma, and mice with *KRAS*G12D, *TP53* and *NOTCH* (KPN) mutations with aggressive, metastatic disease**. (B)** Waterfall plot showing fold difference in copies of *KRAS*G12D detected using ddPCR per µl of DNA extracted from the plasma (cfDNA) and platelets (pDNA) of KP and KPN mice, two weeks after tumor cell implantation, *n* = 5 KP and 15 KPN mice. **(C)** *KRAS*G12D copies detected by ddPCR, shown as copies per µl of DNA extracted from plasma (cfDNA) and platelets (pDNA) of KP, KPN (circle), and KPC (square) mice, compared to the total number of copies from plasma and platelets. *n* = 5 KP, 15 KPN and 6 KPC, datapoints correspond to individual mice, mean ± SEM; $^{**}P < 0.01$; as determined by a paired *t* test. **(D, E)** Representative ddPCR plots showing *KRAS*G12D (blue) in higher abundance in pDNA (top) than in cfDNA (bottom) in two representative mice, **(D)** a KPN mouse and **(E)** a KP mouse. **(F)** Pie charts showing *BRAF*V600E detection in high-risk colonic lesion patients (SSL, *n* = 31) and colonoscopy-screened controls (*n* = 14). Mutant *BRAF* (>3 positive events) was found in 16.1% (5/31) of SSL patients and 0% (0/14) of controls. **(G)** Relative *BRAF*V600E copy number in pDNA vs. cfDNA for five SSL patients with detectable mutant *BRAF*. Data are log2-transformed with a pseudo count of 1. **(H)** ddPCR plot showing *BRAF*V600E (blue) in pDNA (left) and cfDNA (right) for two representative SSL patients. Data are combined. cfDNA, cell free DNA; CRC, colorectal cancer; ddPCR, droplet digital PCR; pDNA, platelet DNA; SSL, sessile serrated lesions; WT, wild type.

Science
AAAS

Supplementary Materials for

Platelets sequester extracellular DNA, capturing tumor-derived and free fetal DNA

Authors: Lauren Murphy[1], Jeanne Inchauspé[1,2], Giampiero Valenzano[3], Pamela Holland[4], Nikolaos Sousos[1,5], Hayley L Belnoue-Davis[6], Rong Li[1], Natalie J. Jooss[1], Camelia Benlabiod[1], Eleanor Murphy[1], Zohar Etzioni[2], Emelie Shepherd[2], Lucy Denly[2], Sujata Biswas[5], Lin Chen[2], Jennifer O'Sullivan[1], Michael P Rimmer[4], Abdullah O. Khan[1], Christina Simoglou Karali[1], Nadia Nasreddin[6], Ian S. Hitchcock[7], Milka Koupenova[8], Skirmantas Kriaucionis[2], Jim R. Hughes[1], Eric O'Neill[3], Manu Vatish[9], Paul Rees[10,11], Simon Leedham[6], Michael Desborough[1,5], Adam J. Mead[1,5], Benjamin Schuster-Böckler*[2], Christopher D. Gregory[4], Bethan Psaila*[1,2,5]

Correspondence to bethan.psaila@ndcls.ox.ac.uk. For computational enquiries: benjamin.schuster-boeckler@ludwig.ox.ac.uk

The PDF file includes:

Supplementary Text
Figs. S1 to S6
Tables S1 to S7
Supplementary Movies S1 to S6

Other Supplementary Materials for this manuscript include the following:

Movies S1 to S6
MDAR Reproducibility Checklist

SUPPLEMENTARY TEXT

15

$$r = \frac{\sum(I1_i - I1_{mean}) \times (I2_i - I2_{mean})}{\sqrt{\sum(I1_i - I1_{mean})^2 \times (I2_i - I2_{mean})^2}}$$

$$R = \frac{\sum I1_i \times I2_i}{\sqrt{\sum(I1_i)^2 \times (I2_i)^2}}$$

Equations used to calculate fluorescence correlation coefficients (Fig. 2H). To quantify signal co-localization between fluorescence channels, the Pearson's correlation coefficient (r) and Mander's overlap coefficient (R) were calculated for each platelet. In both equations $I1_i$ and $I2_i$ represent the fluorescence intensity at pixel *i* in channels 1 and 2, respectively. $I1_{mean}$ and $I2_{mean}$ denote the mean fluorescence intensity across all pixels in the respective channels.

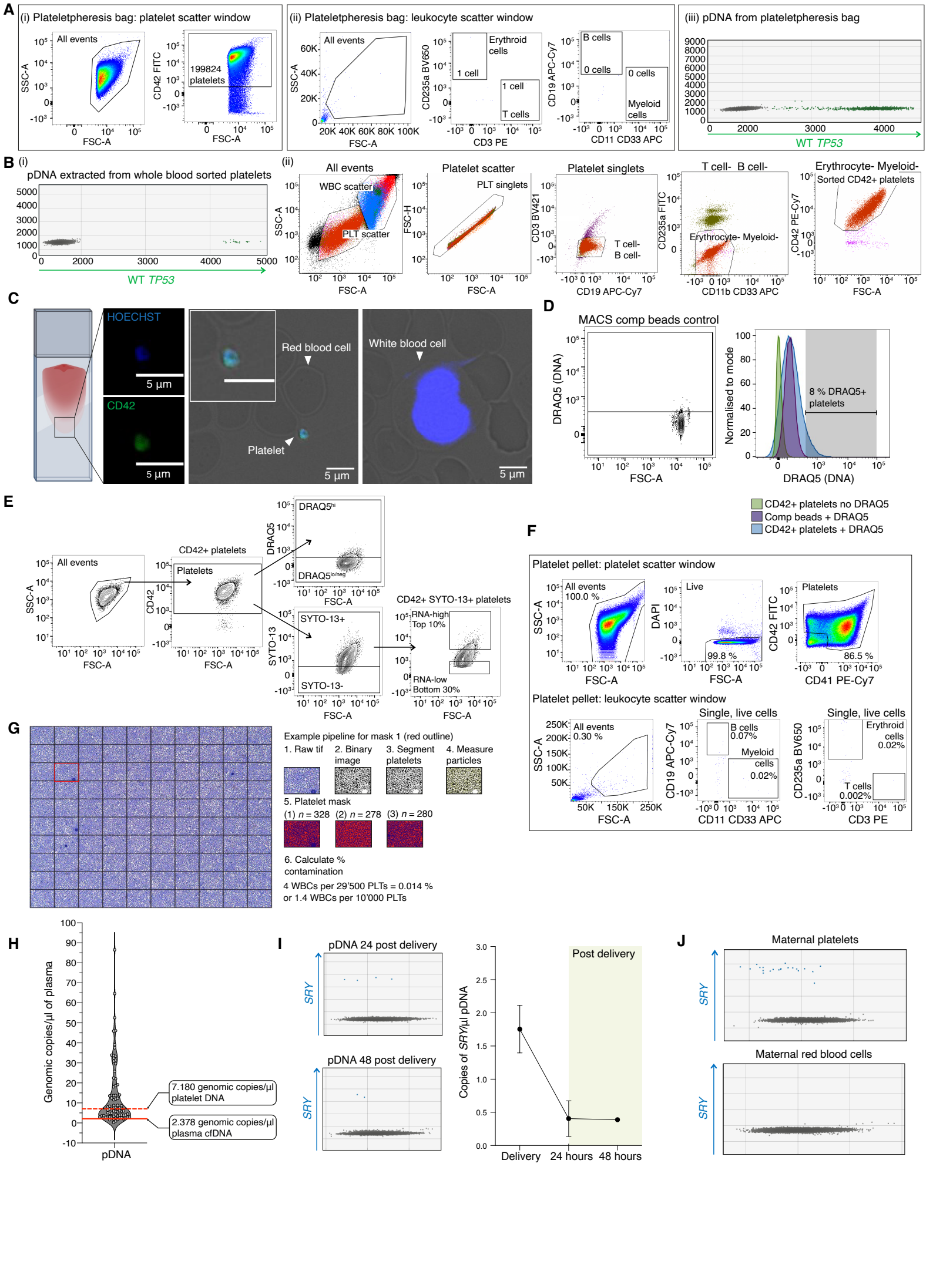

A
(i) Plateletpheresis bag: platelet scatter window
All events
SSC-A
FSC-A
199824 platelets
CD42 FITC
(ii) Plateletpheresis bag: leukocyte scatter window
All events
Erythroid cells
1 cell
T cells
CD235a BV650
CD3 PE
B cells
0 cells
Myeloid cells
CD19 APC-Cy7
CD11 CD33 APC
(iii) pDNA from plateletpheresis bag
WT TP53
B (i)
pDNA extracted from whole blood sorted platelets
WT TP53
(ii)
All events
WBC scatter
PLT scatter
Platelet scatter
PLT singlets
FSC-H
Platelet singlets
CD3 BV421
T cell-
B cell-
CD19 APC-Cy7
T cell- B cell-
CD235a FITC
Erythrocyte- Myeloid-
CD11b CD33 APC
Erythrocyte- Myeloid-
Sorted CD42+ platelets
CD42 PE-Cy7
C
HOECHST
5 µm
CD42
Red blood cell
Platelet
White blood cell
D
MACS comp beads control
DRAQ5 (DNA)
Normalised to mode
8 % DRAQ5+ platelets
E
All events
CD42+ platelets
Platelets
CD42
DRAQ5hi
DRAQ5lo/neg
SYTO-13+
SYTO-13-
SYTO-13
CD42+ SYTO-13+ platelets
RNA-high Top 10%
RNA-low Bottom 30%
F
CD42+ platelets no DRAQ5
Comp beads + DRAQ5
CD42+ platelets + DRAQ5
Platelet pellet: platelet scatter window
All events 100.0 %
Live
99.8 %
DAPI
Platelets
86.5 %
CD41 PE-Cy7
Platelet pellet: leukocyte scatter window
All events 0.30 %
Single, live cells
B cells 0.07%
Myeloid cells 0.02%
Erythroid cells 0.02%
T cells 0.002%
G
Example pipeline for mask 1 (red outline)
1. Raw tif
2. Binary image
3. Segment platelets
4. Measure particles
5. Platelet mask
(1) n = 328
(2) n = 278
(3) n = 280
6. Calculate % contamination
4 WBCs per 29'500 PLTs = 0.014 %
or 1.4 WBCs per 10'000 PLTs
H
Genomic copies/µl of plasma
7.180 genomic copies/µl platelet DNA
2.378 genomic copies/µl plasma cfDNA
pDNA
I
pDNA 24 post delivery
pDNA 48 post delivery
SRY
Copies of SRY/µl pDNA
Post delivery
Delivery
24 hours
48 hours
J
Maternal platelets
Maternal red blood cells
SRY

Fig S1. Detection of DNA fragments and free fetal DNA in circulating blood platelets. **(A)** DNA was extracted from three healthy donor plateletpheresis concentrates. Flow cytometry confirms high platelet purity with minimal blood cell contamination. Plots show (i) platelet and (ii) leukocyte scatter with absolute cell counts. (iii) ddPCR detects wild-type (WT) *TP53* gene copies in platelets. **(B)** (i) ddPCR quantification of WT *TP53* gene copies from DNA extracted from 20.7 x 10^6 CD42+ platelets FACS-isolated from whole blood, following (ii) rigorous gating to exclude contaminating nucleated blood cell types (B cells, T cells and myeloid cells) and erythrocytes. *n* = 1 healthy donor. **(C)** Peripheral blood film from a healthy donor stained with CD42 AF488 (green) for platelets and Hoechst (blue) for DNA. Platelets show a Hoechst-positive signal. Red blood cells and white blood cells are also indicated. White box highlights a magnified region, scale bars represent 5 µm. Representative image acquired using a Leica SPE. **(D)** Representative flow cytometric analysis of MACS compensation beads stained with DRAQ5 to control for DRAQ5 non-specific binding (*n* = 1 healthy donor). Right, thresholding to identify strongly DRAQ5+ platelets (*n* = 20 healthy donors, blue; concatenated into a single histogram), defined by fluorescence exceeding that of compensation beads (*n* = 1 donor, purple). **(E)** Flow cytometric gating strategy for defining newly produced (RNA-high) and older (RNA-low) platelets. 'Young' platelets are identified as being within the top 10% of SYTO-13 staining, while 'old' are within the bottom 30%. *n* = 10 healthy donors, concatenated data shown. **(F)** Flow cytometric analysis of a representative platelet pellet from a healthy donor (*n* = 1 donor) confirming high platelet yield with minimal leukocyte and red blood cell contamination. Platelet (top) and leukocyte (bottom) scatter windows are shown, using thresholds of 1000 for platelets and 5000 for leukocytes and red blood cells. **(G)** Cytospin with Wright-Giemsa staining and leukocyte contamination quantification in a representative colorectal patient platelet pellet (*n* = 1 patient). Imaged at 40X using an Olympus BX51 fluorescent microscope. **(H)** Violin plot showing DNA yield from platelet pellets and platelet-depleted plasma, measured as genomic equivalents per µl of plasma. *n* = 76 donors, including non-cancer controls, patients with pre-malignant serrated polyps and gastrointestinal carcinoma. Each data point represents one patient. Dashed line indicates the median DNA yield from platelet pellets (7.180 genomic copies/µl of platelet-rich plasma), while solid line marks the median yield of DNA from paired platelet-depleted plasma (cfDNA, 2.378 genomic copies/µl of plasma). **(I)** Top, representative ddPCR detection of the Y-chromosome gene *SRY* in maternal platelets 24 and 48 hours post-cesarean delivery of a male infant. Bottom, mean *SRY* copies ± SEM, in maternal platelets at delivery (*n* = 9 donors), 24 hours (*n* = 5) and 48 hours post-delivery (*n* = 2). **(J)** Representative ddPCR showing detection of the Y-chromosome gene *SRY* in maternal platelets, but not red blood cells sampled from mothers of male offspring prior to delivery. ddPCR, droplet digital PCR; FACS, fluorescence activated cell sorting; pDNA, platelet DNA; *SRY*, sex-determining region Y; WT, wild type.

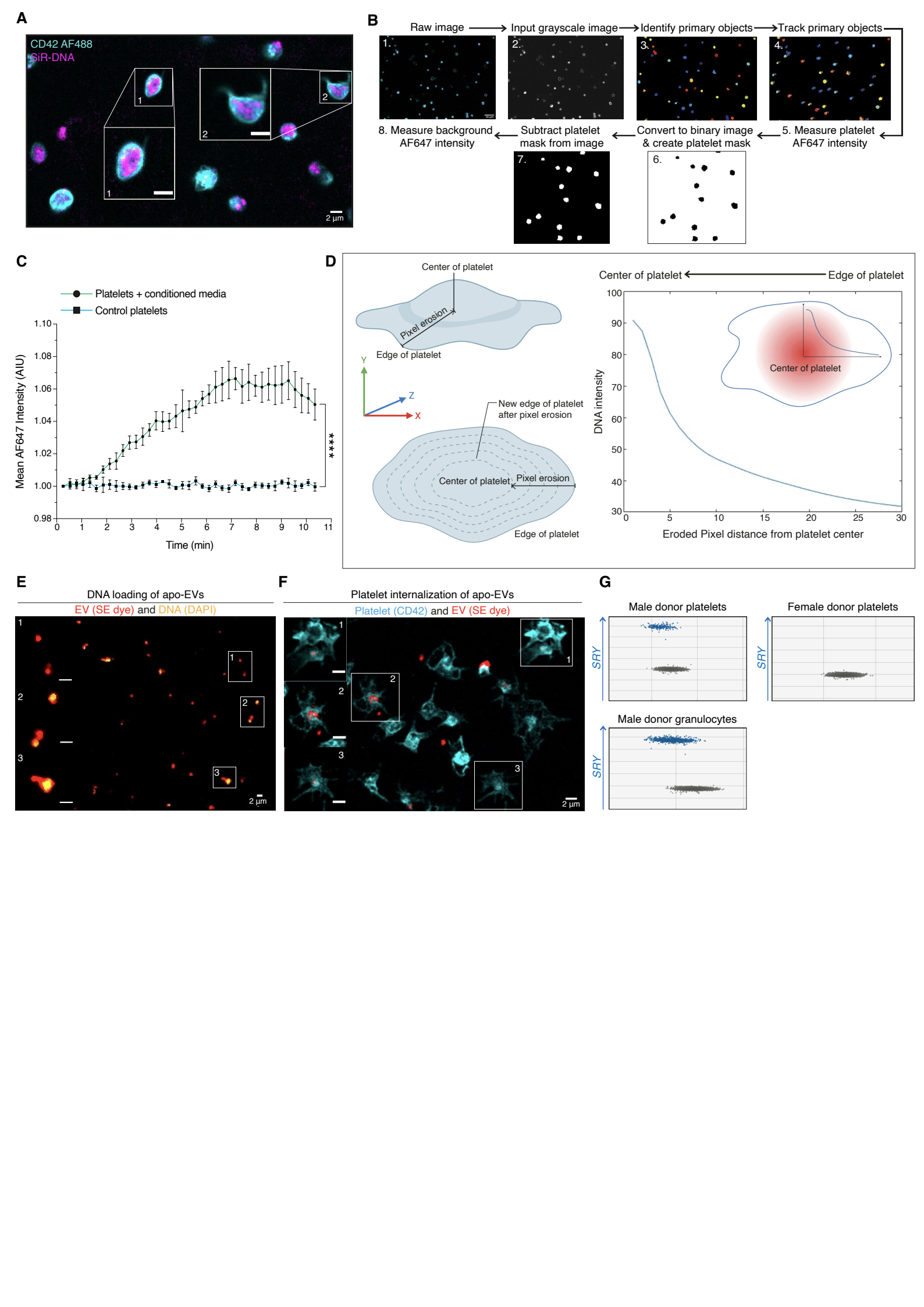

A
CD42 AF488
SiR-DNA
2 µm
B
Raw image
Input grayscale image
Identify primary objects
Track primary objects
1.
2.
3.
4.
5. Measure platelet AF647 intensity
Convert to binary image & create platelet mask
Subtract platelet mask from image
8. Measure background AF647 intensity
6.
7.
C
Platelets + conditioned media
Control platelets
Mean AF647 Intensity (AIU)
Time (min)
****
D
Center of platelet
Pixel erosion
Edge of platelet
New edge of platelet after pixel erosion
Center of platelet
Edge of platelet
DNA intensity
Eroded Pixel distance from platelet center
E
DNA loading of apo-EVs
EV (SE dye) and DNA (DAPI)
2 µm
F
Platelet internalization of apo-EVs
Platelet (CD42) and EV (SE dye)
2 µm
G
Male donor platelets
Female donor platelets
Male donor granulocytes
SRY

Fig S2. Platelet sequestration of DNA released by nucleated cells. (A) COLO205 colorectal carcinoma cells were labeled with SiR-DNA (magenta), washed twice and co-incubated with CD42 AF488 labeled healthy donor platelets (cyan). White box highlights COLO205-derived DNA in platelets. Images acquired on a Zeiss Spinning Disk confocal at 63X magnification, representative platelets shown. **(B)** CellProfiler method to quantify fluorescently labeled DNA uptake by platelets over time: (1-2) convert raw images to grayscale, (3) segment platelets, (4) track individual platelets over 10 minutes, (5) calculate average platelet DNA (AF647) signal per frame, and (6-8) subtract background intensity. **(C)** Time-course quantification of platelet DNA fluorescence intensity presented as mean ± SD. ****$P <$ 0.0001; as determined by a Wilcoxon signed-rank test. Tracking of five randomly selected platelets incubated with control media (n = 5 platelets) or media conditioned by NUCLEAR-ID-labeled COLO205 cells (n = 5 platelets). AF647 signal normalized to frame 1. **(D)** Left, schematic outlining the method used to measure DRAQ5 pixel intensity in CD62P labeled, healthy donor platelets spread on collagen. CD62P was used to generate a 3D platelet mask which was subsequently eroded pixel-by-pixel towards the center of the platelet. Intensities along the X, Y, and Z planes were calculated. Right, pixel intensity (y axis) was plotted against distance from platelet center (x axis). DNA (DRAQ5) signal is strongest at the center of the platelet. Data collected from n = 1 healthy donor platelet. **(E)** Representative BL2 cell derived apo-EVs labeled with an amine-reactive membrane dye (CF658, red), stain positive for the DNA stain, DAPI (yellow). Imaged using a ZEISS LSM900, 63X magnification, scale bars represent 2 μm. **(F)** Following incubation with labeled EVs, platelets were stained with CD42 AF488 (cyan). EVs (red) were visualized in platelets, confirming platelet uptake of apo-EVs. White boxes show magnified regions, scale bars represent 2 μm. **(G)** Representative ddPCR detection of the Y-chromosome gene *SRY* in male donor platelets and granulocytes but not in female donor platelets. AIU, Arbitrary intensity units; BL2, Burkitt's lymphoma cells; ddPCR, droplet digital PCR; SE, succinimidyl ester; *SRY*, sex-determining region Y.

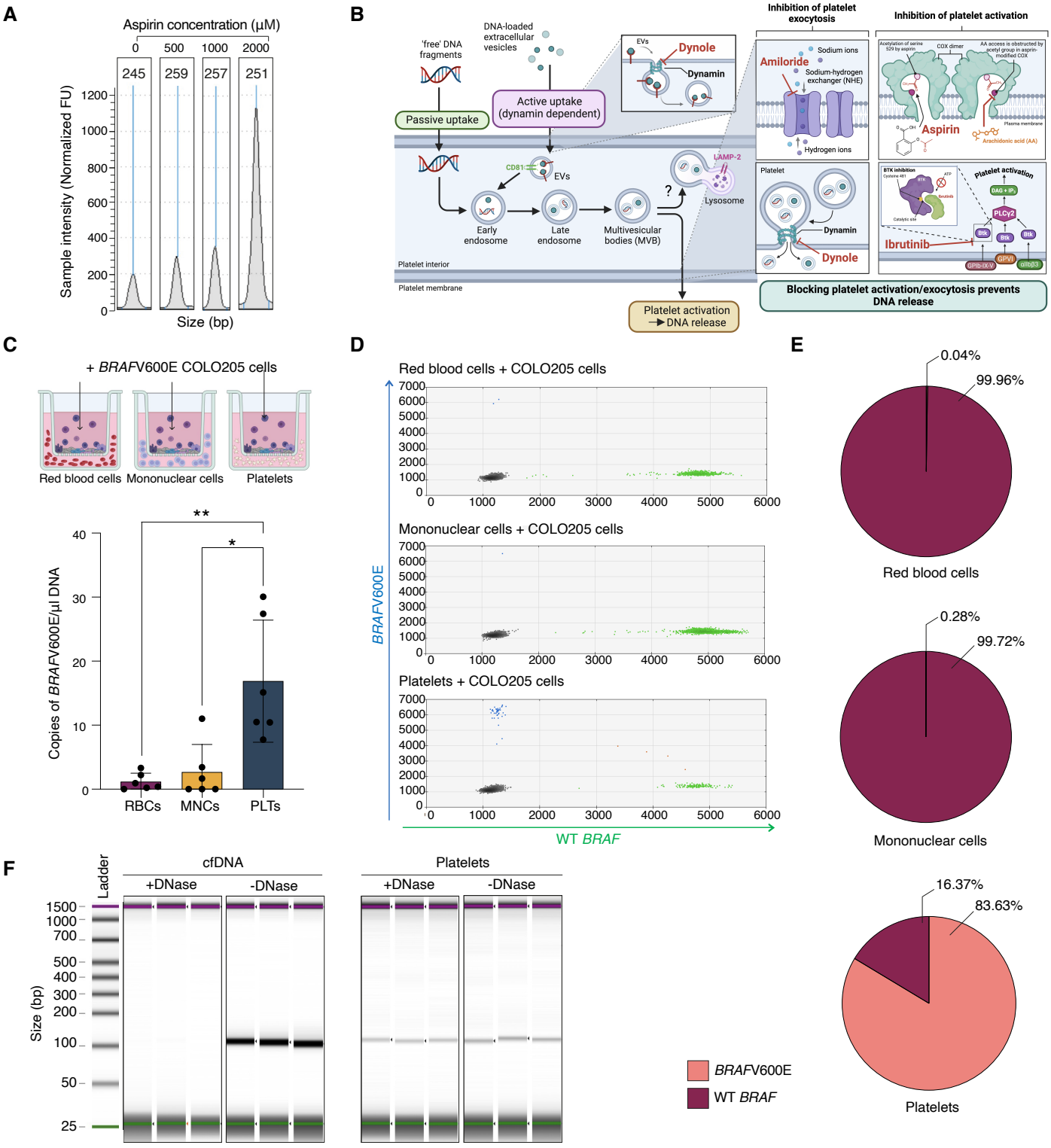

A
Aspirin concentration (μM)
0
500
1000
2000
245
259
257
251
Sample intensity (Normalized FU)
Size (bp)
B
'free' DNA fragments
DNA-loaded extracellular vesicles
Passive uptake
Active uptake (dynamin dependent)
EVs
Dynole
Dynamin
CD81
Early endosome
Late endosome
Multivesicular bodies (MVB)
LAMP-2
Lysosome
Platelet interior
Platelet membrane
Platelet activation → DNA release
Inhibition of platelet exocytosis
Amiloride
Sodium ions
Sodium-hydrogen exchanger (NHE)
Hydrogen ions
Platelet
Inhibition of platelet activation
COX dimer
Aspirin
Arachidonic acid (AA)
Plasma membrane
Platelet activation
DAG + IP3
PLCγ2
Btk
Ibrutinib
GPVI
αIIbβ3
Blocking platelet activation/exocytosis prevents DNA release
C
+ BRAFV600E COLO205 cells
Red blood cells
Mononuclear cells
Platelets
Copies of BRAFV600E/μl DNA
**
*
RBCs
MNCs
PLTs
D
Red blood cells + COLO205 cells
Mononuclear cells + COLO205 cells
Platelets + COLO205 cells
BRAFV600E
WT BRAF
E
0.04%
99.96%
Red blood cells
0.28%
99.72%
Mononuclear cells
16.37%
83.63%
Platelets
F
Ladder
cfDNA
+DNase
-DNase
Platelets
+DNase
-DNase
Size (bp)
1500
1000
700
500
400
300
200
100
50
25
BRAFV600E
WT BRAF

Fig S3. Mechanisms of DNA trafficking by platelets and detection of cancer cell-derived DNA in platelets. (A) Representative electrophoresis showing recovery of 260 bp synthetic DNA fragments from platelets treated with increasing concentrations of aspirin (0, 500, 1000 and 2000 μM), *n* = 3 independent experiments. **(B)** Schematic illustrating DNA trafficking mechanisms. Uptake of synthetic, non-membrane-encapsulated DNA was unaffected by inhibitors, while DNA-loaded vesicle uptake was reduced by dynamin inhibition (Dynole), indicating distinct uptake pathways. Inhibitors of platelet activation (aspirin, ibrutinib) and exocytosis (Dynole, amiloride) increased DNA yield from platelet pellets by blocking DNA release. Inhibitor mechanisms are shown. **(C)** Top, schematic showing co-culture of COLO205 cells with red blood cells, mononuclear cells and platelets. Bottom, quantification of *BRAF*V600E in DNA extracted from each cell type following co-culture with COLO205 cells. Data points show mean ± SD, each point represents 1 co-culture experiment, *n* = 6 replicate wells from three independent experiments, **P* < 0.05; ***P* < 0.01; as determined by a Mann-Whitney *U* test. **(D)** Representative ddPCR for *BRAF*V600E in DNA isolated from red blood cells, mononuclear cells and platelets following incubation in COLO205 cell conditioned media. **(E)** Percentage detection of *BRAF* wild-type and mutant alleles in red blood cells, mononuclear cells and platelets. Data collected from *n* = 6 replicate wells from three independent incubation experiments. **(F)** Representative electrophoresis showing recovery of synthetic, 128 bp DNA fragments from healthy donor derived platelets after treatment with or without DNase, *n* = 3 independent experiments. MNCs, mononuclear cells; PLTs, platelets; RBCs, red blood cells; WT, wild type.

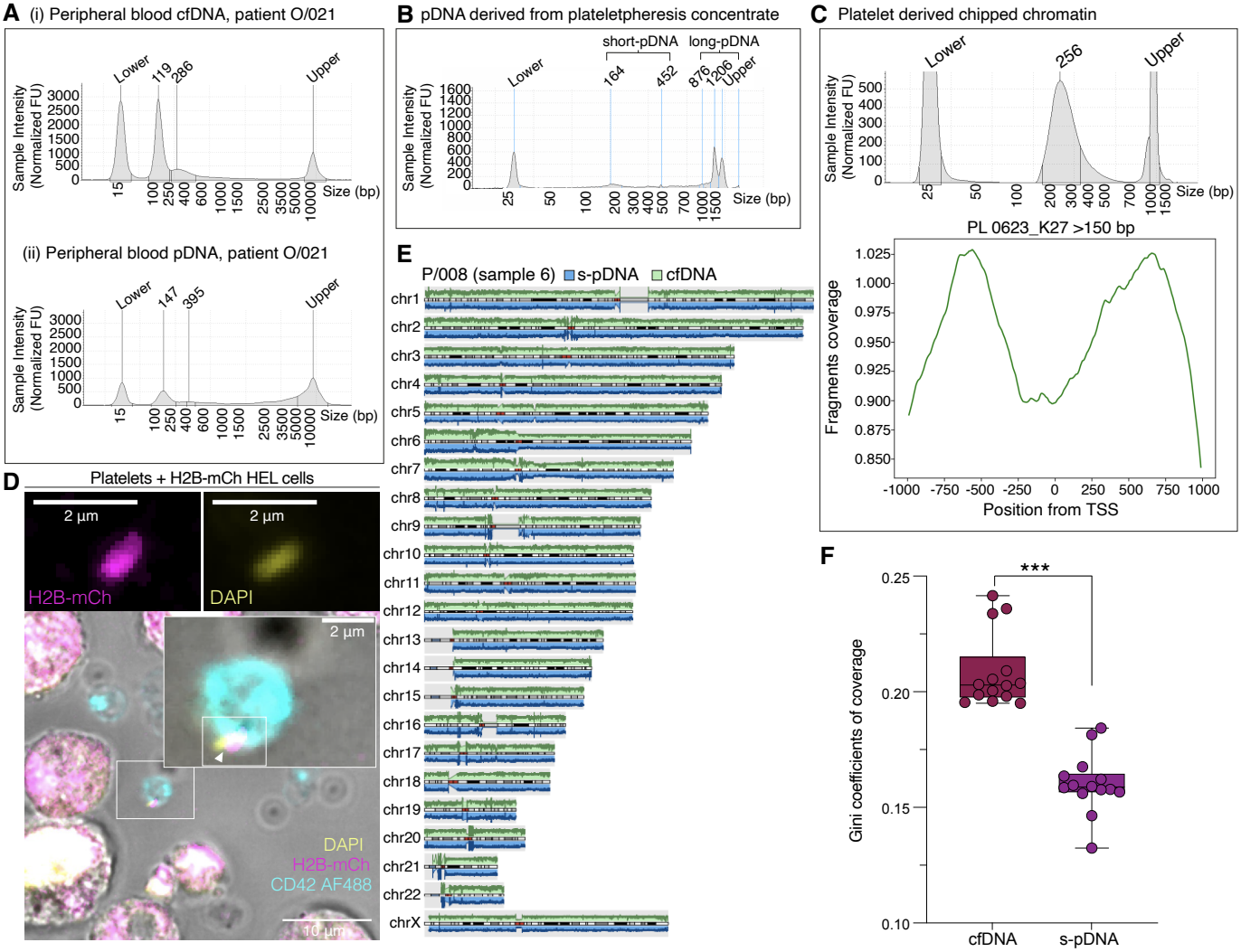

A
(i) Peripheral blood cfDNA, patient O/021
Lower
119
286
Upper
Sample Intensity (Normalized FU)
Size (bp)
(ii) Peripheral blood pDNA, patient O/021
Lower
147
395
Upper
B
pDNA derived from plateletpheresis concentrate
short-pDNA
long-pDNA
Lower
164
452
876
1206
Upper
C
Platelet derived chipped chromatin
Lower
256
Upper
PL 0623_K27 >150 bp
Fragments coverage
Position from TSS
D
Platelets + H2B-mCh HEL cells
2 µm
H2B-mCh
DAPI
CD42 AF488
10 µm
E
P/008 (sample 6)
s-pDNA
cfDNA
chr1
chr2
chr3
chr4
chr5
chr6
chr7
chr8
chr9
chr10
chr11
chr12
chr13
chr14
chr15
chr16
chr17
chr18
chr19
chr20
chr21
chr22
chrX
F
***
Gini coefficients of coverage
cfDNA
s-pDNA

Fig S4. Platelets capture fragments of DNA that map across the human genome, including DNA fragments from cancer cells. (A) Representative electrophoresis of DNA extracted from (i) plasma and (ii) peripheral blood platelets, showing peaks at ~150 bp and nucleosomal footprints. **(B)** Representative electrophoresis of platelet DNA extracted from one of three plateletpheresis samples showing a peak at ~160 bp as well as larger DNA fragments, *n* = 3 plateletpheresis donors. **(C)** Top, representative electrophoresis of a H3K27ac ChIPmentation DNA library from platelet chromatin. Bottom, coverage of the H3K27ac ChIP-seq reads at the TSS, for nucleosomal reads (bioinformatically size selected to >= 150 bp). The typical low coverage at the TSS, flanked by regions of higher coverage, suggests open chromatin with surrounding nucleosomes marked by H3K27ac at the TSS. This result suggests DNA in platelets is in chromatin form and contains promoter signal. The signal was smoothed with a Savitzky-Golay filter and repeated in *n* = 2 plateletpheresis donors. **(D)** Representative image of healthy donor platelets (CD42 AF488, cyan) incubated with H2B-mCh HEL cells genetically engineered to express mCherry-tagged histones (magenta). Arrow shows platelet sequestration of tumor cell-derived histones (magenta) and DNA (DAPI, yellow). White box shows magnified region, scale bars represent 2 μm, imaged using a Zeiss Spinning Disk Confocal with a 63X oil immersion objective. **(E)** Chromosome mapping of short platelet DNA and paired cfDNA for a representative patient with pancreatic adenocarcinoma (P/008, sample 6, *n* = 1). **(F)** s-pDNA fragments have more even chromosome coverage, as indicated by a significantly lower Gini index compared to cfDNA as calculated by a Wilcoxon signed-rank test, ***$P < 0.001$; *n* = 14 patients with gastrointestinal carcinoma. In the box plot, the center line represents the median, whiskers indicate the minimum and maximum values, and dots represent individual patients. cfDNA, cell free DNA; pDNA, platelet DNA; s-pDNA, short platelet DNA; TSS, transcription start sites.

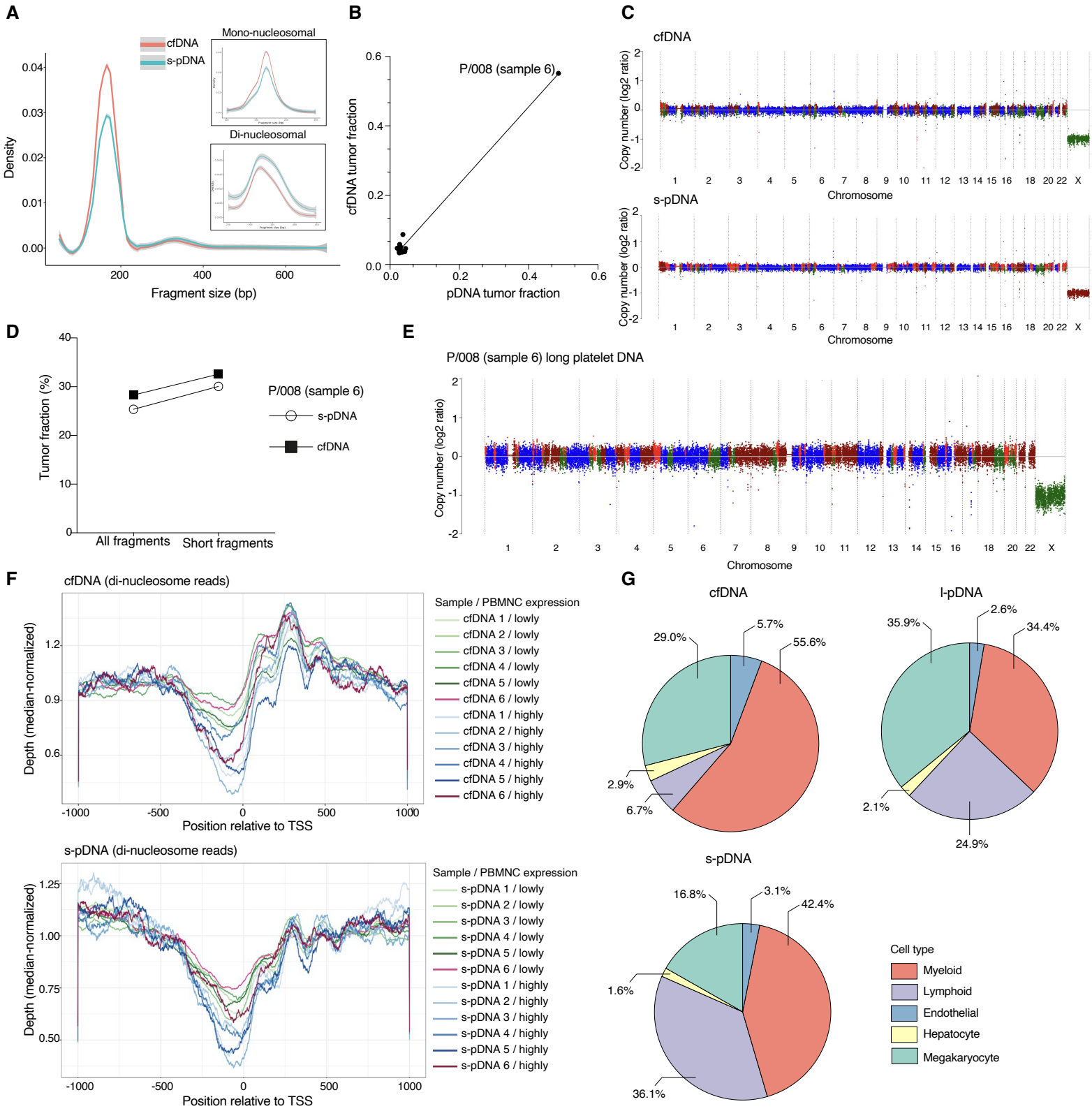

A
cfDNA
s-pDNA
Mono-nucleosomal
Di-nucleosomal
Density
Fragment size (bp)
B
P/008 (sample 6)
cfDNA tumor fraction
pDNA tumor fraction
C
cfDNA
s-pDNA
Copy number (log2 ratio)
Chromosome
D
Tumor fraction (%)
P/008 (sample 6)
s-pDNA
cfDNA
All fragments
Short fragments
E
P/008 (sample 6) long platelet DNA
Copy number (log2 ratio)
Chromosome
F
cfDNA (di-nucleosome reads)
Depth (median-normalized)
Position relative to TSS
Sample / PBMNC expression
cfDNA 1 / lowly
cfDNA 2 / lowly
cfDNA 3 / lowly
cfDNA 4 / lowly
cfDNA 5 / lowly
cfDNA 6 / lowly
cfDNA 1 / highly
cfDNA 2 / highly
cfDNA 3 / highly
cfDNA 4 / highly
cfDNA 5 / highly
cfDNA 6 / highly
s-pDNA (di-nucleosome reads)
Depth (median-normalized)
Position relative to TSS
Sample / PBMNC expression
s-pDNA 1 / lowly
s-pDNA 2 / lowly
s-pDNA 3 / lowly
s-pDNA 4 / lowly
s-pDNA 5 / lowly
s-pDNA 6 / lowly
s-pDNA 1 / highly
s-pDNA 2 / highly
s-pDNA 3 / highly
s-pDNA 4 / highly
s-pDNA 5 / highly
s-pDNA 6 / highly
G
cfDNA
29.0%
5.7%
55.6%
2.9%
6.7%
l-pDNA
35.9%
2.6%
34.4%
2.1%
24.9%
s-pDNA
16.8%
3.1%
42.4%
1.6%
36.1%
Cell type
Myeloid
Lymphoid
Endothelial
Hepatocyte
Megakaryocyte

Fig S5. Platelet DNA analysis reveals copy number variations and cell-of-origin. (A) Plot showing significantly higher frequency of di-nucleosomal fragments (fragments > 250 bp) in s-pDNA than cfDNA (P < 0.0005 for all samples as determined by a chi-square test of independence). n = 14 patients with gastrointestinal carcinoma, insets show zoomed in mono- and di-nucleosomal peaks. The standard error of the mean is shown in gray. **(B)** CNA-based estimates of tumor fraction in cfDNA and pDNA are highly correlated, n = 14 patients with gastrointestinal carcinoma, each dot represents one patient. **(C)** Deviation from median coverage in 100 kbp windows across chromosomes for cfDNA and s-pDNA for a patient with colorectal carcinoma who had a curative right hemicolectomy prior to blood sampling (n = 1 patient). **(D)** Estimated tumor fraction increases after computationally selecting DNA fragments smaller than 150 bp for both s-pDNA and cfDNA for P/008 (sample 6, n = 1). **(E)** Copy number alterations were not observed in long platelet DNA for the same patient (P/008, sample 6, n =1). **(F)** Read depth distribution around transcription start sites of genes highly (TPM >15, blue) or lowly (TPM <15, green) expressed in peripheral blood mononuclear cells for cfDNA (top) and s-pDNA (bottom) di-nucleosome-length reads. n = 6 donors with gastrointestinal carcinoma, depth per position per sample was normalized to the median read depth across all genes in that expression category. **(G)** Cell type deconvolution of low-input whole genome DNA methylation data to compare cell-of-origin of cfDNA (n = 10 healthy donors), long platelet DNA (n = 6 healthy donors) and short platelet DNA (n = 6 healthy donors). Long and short DNA were from matched donors. 'Lymphoid' contributions include B, T, and NK cells, while 'Myeloid' contributions include granulocytes, monocytes, and erythrocytes. CNA, copy number analysis; kbp, kilobase pair; NK, natural killer; PBMNC, peripheral blood mononuclear cell; TPM, transcripts per million; TSS, transcriptional start site.

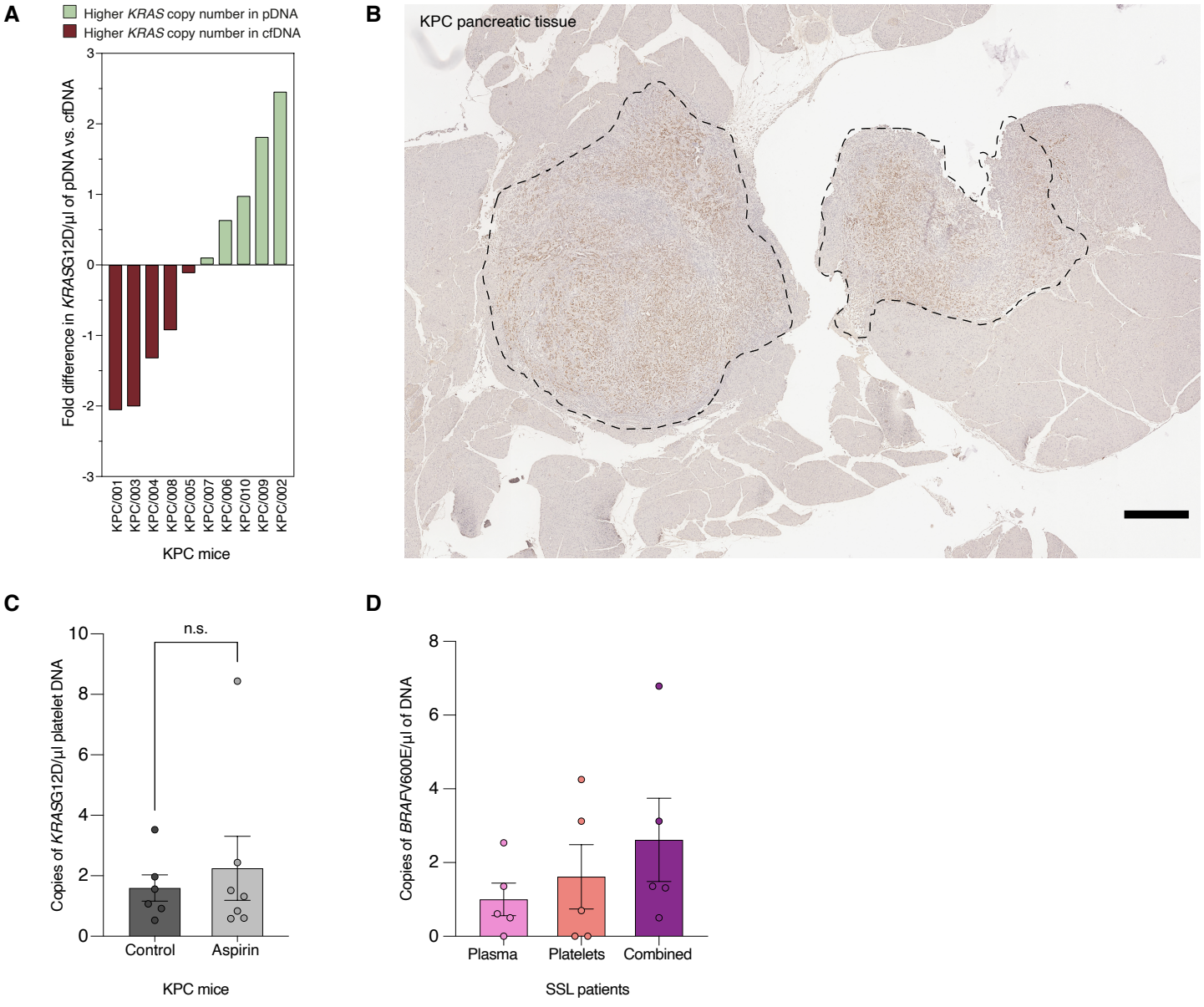

A
Higher KRAS copy number in pDNA
Higher KRAS copy number in cfDNA
Fold difference in KRASG12D/µl of pDNA vs. cfDNA
3
2
1
0
-1
-2
-3
KPC/001
KPC/003
KPC/004
KPC/008
KPC/005
KPC/007
KPC/006
KPC/010
KPC/009
KPC/002
KPC mice
B
KPC pancreatic tissue
C
n.s.
Copies of KRASG12D/µl platelet DNA
10
8
6
4
2
0
Control
Aspirin
KPC mice
D
Copies of BRAFV600E/µl of DNA
8
6
4
2
0
Plasma
Platelets
Combined
SSL patients

Fig S6. DNA abundance in platelets and plasma of mice with pancreatic cancer. (A) Waterfall plot showing fold difference in copies of *KRAS*G12D detected using ddPCR per µl of DNA extracted from the plasma (cfDNA) and platelets (pDNA) of KPC mice, two weeks after tumor cell implantation, *n* = 10 mice, each bar represents one mouse. **(B)** Representative image showing p53 immunohistochemical staining of KPC pancreatic tissue, two weeks post engraftment. Outlined area highlights regions of contained p53 expression surrounded by healthy p53neg tissue. Scale bar represents 500 µm. **(C)** Copies of *KRAS*G12D detected in DNA extracted from the platelets of KPC mice, normalized to cfDNA copies per mouse, to account for aspirin's effect on tumor growth. Mice were treated with aspirin (10 mg/kg) or control for two weeks, starting four days after tumor cell implantation. >1 indicates more *KRAS*G12D copies in platelets compared to paired cfDNA. Individual points represent one mouse with mean ± SEM, *n* = 6 control mice and *n* = 7 aspirin treated mice, n.s., not significant as determined by paired *t* test. **(D)** ddPCR quantification of mutant *BRAF*V600E copies per µl of DNA from platelet-poor plasma and platelets in five patients with SSLs, where mutant *BRAF* was detected in either patient cfDNA or pDNA (*n* = 5 SSL patients) . The combined cfDNA and platelet signal is also shown. Each datapoint represents one patient, mean ± SEM. ddPCR, droplet digital PCR; KPC, LSL-*Kras*G12D, LSL-*Trp53*R172H, *Pdx1*Cre; SSL, sessile serrated lesions.

SUPPLEMENTARY TABLES

Patient ID	Blood collection tube	Age (years)	Sex	Platelet count ($x10^9$/L)
NC/001	Streck	35	M	N/A
NC/003	Streck	63	M	303
NC/004	Streck	66	F	211
NC/005	Streck	65	M	330
NC/006	Streck	53	F	282
NC/007	Streck	28	F	200
NC/008	Streck	42	M	343
NC/009	Streck	61	M	255
NC/010	Streck	41	F	398
NC/011	Streck	69	F	216
NC/012	Streck	28	M	270
NC/013	Streck	47	F	398
NC/015	Streck	72	M	N/A
NC/018	Streck	81	M	137

Table S1: Clinical information for the control cohort (*n* = 14, including patients with ulcerative colitis, Crohn's disease and individuals on the bowel cancer screening program).

F, female; M, male; N/A, not available; NC, non-cancer control

Patient ID	Blood collection tube	Age (years)	Sex	Platelet count (x10^9/L)	Diagnosis
SSL/001*	Streck	43	F	260	Confirmed SSL and on surveillance
SSL/002*	Streck	38	F	N/A	Confirmed SSL and on surveillance
SSL/003*	Streck	37	M	274	Confirmed SSL and on surveillance
SSL/004	Streck	73	M	205	Confirmed SSL and on surveillance
SSL/005	Streck	41	M	92	Confirmed SSL and on surveillance for SSLs as well as previous surgery for CRC
SSL/006*	Streck	52	F	351	Confirmed SSL and on surveillance
SSL/007	Streck	75	M	270	Confirmed SSL and on surveillance
SSL/007.2	Streck	76	M	N/A	Confirmed SSL and on surveillance
SSL/008	Streck	38	M	N/A	Surveillance after previous polyps, family history of CRC and SSL
SSL/009*	Streck	35	F	N/A	Confirmed SSL and on surveillance
SSL/010	Streck	43	F	188	Confirmed SSL and on surveillance
SSL/012	Streck	44	F	317	Not confirmed SSL but on surveillance
SSL/013	Streck	75	F	348	Confirmed SSL and on surveillance
SSL/018	Streck	41	F	276	Confirmed SSL and on surveillance
SSL/019	Streck	48	F	208	Confirmed SSL and on surveillance
SSL/022	Streck	43	F	N/A	Confirmed SSL and on surveillance
SSL/024	Streck	40	F	246	Confirmed SSL and on surveillance
SSL/025	Streck	43	F	N/A	Confirmed SSL and on surveillance
SSL/026	Streck	43	M	N/A	Confirmed SSL and on surveillance
SSL/027	Streck	70	F	N/A	Confirmed SSL and on surveillance
SSL/028	Streck	73	F	N/A	Confirmed SSL and on surveillance
SSL/029	Streck	43	M	N/A	Confirmed SSL and on surveillance
SSL/030	Streck	42	M	N/A	Confirmed SSL and on surveillance
SSL/30.2	Streck	43	M	215	Confirmed SSL and on surveillance
SSL/031	Streck	62	F	229	Confirmed SSL and on surveillance
SSL/032	Streck	43	M	N/A	Confirmed SSL and on surveillance
SSL/033	Streck	25	F	N/A	Familial adenomatous polyposis and on surveillance
SSL/034	Streck	41	M	226	Confirmed SSL and on surveillance
SSL/035	Streck	40	M	251	Confirmed SSL and on surveillance
SSL/037	Streck	44	F	N/A	Confirmed SSL and on surveillance
SSL/038	Streck	45	M	N/A	Confirmed SSL and on surveillance
SSL/039	Streck	41	F	N/A	Confirmed SSL and on surveillance
SSL/040	Streck	56	F	278	Confirmed SSL and on surveillance
SSL/041	Streck	59	M	251	Confirmed SSL and on surveillance

Table S2: Clinical information for patients with pre-malignant sessile serrated lesions (*n* = 34).

* SSL patients where *BRAF*V600E was detected in either cfDNA or pDNA
CRC, colorectal cancer; F, female; M, male; N/A, not available; SSL, sessile serrated lesions

Patient ID	Blood collection tube	Cancer type	Platelet count (x10^9/L)	Tumor information (location, size)	TNM staging	Additional pathologic features	Identified mutations	Therapy
C/024	Streck	Colorectal	332	Ascending colon, caecum with intramural lymphatic invasion. Tumor size: 5.5 cm	T4a N1a Mx	N/A	None identified	N/A
C/025	Streck	Colorectal	248	Sigmoid cancer with liver metastasis	T3 N2 M1	N/A	*TP53* c.578A>G p.(His193Arg)	4 cycles of chemotherapy (oxaliplatin and capecitabine)
C/027	EDTA	Colorectal	235	Transverse colon	T3 N0 M0	N/A	*TP53* c.733G>A p.(Gly2455Ser)	N/A
C/028	EDTA	Colorectal	323	Ascending colon	T2 N1 M0	N/A	*TP53* c.659A>G p.(Tyr220Cys)	N/A
C/029	EDTA	Colorectal	183	Rectosigmoid tumor	T4a N1 Mx	pT4a pN1b Ly1 V1 R0	*TP53* c.742C>T p.(Arg248Trp). *KRAS* c.37G>T p.(Gly13Cys)	N/A
C/031	Streck	Colorectal	317	Ascending colon. Tumor size: 22 mm	T2 N0 Mx	pT2 pN0 Ly0 V0 R0	*KRAS*: c.34G>T p.(Gly12Cys). *PIK3CA*: c.1258T>C p.(Cys420Arg).*TP53*: c.691A>C p.(Thr231Pro)	N/A
O/030	Streck	Esophageal	193	Proximal/mid oesophagus. Tumor size: 3.5 cm	T2 N1 M0	R1 pT3 L1 V0 Pn0 N1 [2/19] M0	None identified	2 cycles of neoadjuvant chemotherapy (cisplatin and fluorouracil) prior to surgery
O/019	EDTA	Esophageal	225	Oesophagogastric junction. Tumor size: 63 mm (30 mm above + 33 mm below)	T1a N0 Mx	R0 ypT1a L0 V0 Pn0 N0	None identified	4 cycles of neoadjuvant FLOT chemotherapy, 2 months prior to blood sampling

Table S3: Clinical information for patients with gastrointestinal carcinoma (*n* = 15).

FLOT, Combination of chemotherapy drugs: docetaxel, oxaliplatin, 5-fluorouracil and leucovorin; GOJ, gastro-esophageal junction

Patient ID	Blood collection tube	Cancer type	Platelet count (x10^9/L)	Tumor information (location, size)	TNM staging	Additional pathologic features	Identified mutations	Therapy
O/023	EDTA	Esophageal	261	Gastric cardia just below GOJ. Tumor size: 45 mm	T4a N2 M1	R1 ypT4a L1 Pn1 N2 (4/35) M1	None identified	4 cycles of neoadjuvant FLOT chemotherapy 1 month prior to blood sampling
O/024	Streck	Esophageal	189	Tumor at GOJ, size: 30 mm	T3 N0 M0	R0 ypT3 L0 V0 Pn0 N0 (0/22) M0	None identified	Post neoadjuvant FLOT chemotherapy and radiotherapy after blood sampling
O/025	Streck	Esophageal	N/A	N/A	N/A		N/A	N/A
O/026	Streck	Esophageal	270	Tumor at lower 3rd distal oesophagus and GOJ. Tumor size: 30 mm x 45 mm	T3 N2 M0	R0 ypT3 L1 V0 Pn1 N2	None identified	4 cycles of neoadjuvant FLOT and 5FU, 3 months prior to blood sampling
O/027	Streck	Esophageal	254	GOJ. No tumor present, regression from chemotherapy	Original staging was T3 before chemotherapy	R0 ypT0 L0 V0 Pn0 N0 (0/40) M0	None identified	Chemotherapy finished 11 weeks prior to blood sampling
O/028	Streck	Esophageal	273	Tumor at GOJ, size: 30 x 35 mm	T3 N0 M0 at time of bloods. T3 N3 M0 after surgery	N/A	None identified	N/A
P/009	Streck	Pancreatic	243	Distal pancreas. Tumor size: 20 mm	T1 N0 Mx	N/A	None identified	N/A

Table S3: Clinical information for patients with gastrointestinal carcinoma (*n* = 15) continued.

FLOT, Combination of chemotherapy drugs: docetaxel, oxaliplatin, 5-fluorouracil and leucovorin; GOJ, gastro-esophageal junction

Patient ID	Blood collection tube	Cancer type	Platelet count ($x10^9$/L)	Tumor information (location, size)	TNM staging	Identified mutations	Therapy
C/023	Streck	Colorectal	232	Caecum	T4 N0 M0	Loss of *MLH1,PMS2* IHC staining	Surgery and curative right hemicolectomy
C/026	EDTA	Colorectal	207	Rectum	T4a N1 M0	*KRAS* c.35G>A p.(Gly12Asp)	Surgery & neoadjuvant chemoradiotherapy
O/020	EDTA	Esophageal	249	Distal oesophagus	T2 N1 M0	None identified	Surgery and neoadjuvant chemoradiotherapy
O/021	EDTA	Esophageal	199	Distal oesophagus	T2 N0 M0	None identified	Surgery and neoadjuvant chemotherapy
O/022	EDTA	Esophageal	304	Gastric antrum	T4a N0 M0	None identified	Surgery
P/008*	Streck	Pancreatic	266	Large 11 cm mass involving pancreatic tail, spleen, stomach and transverse colon	T4 N1 M0	None identified	No therapy prior to blood sampling
P/017	Streck	Pancreatic	205	Pancreatic ductal adenocarcinoma	pT3 N1 (2/3) L1V1	None identified	Curative intent surgery
Combat CRC 008	Streck	Colorectal	247	Colon (ascending)	T3 N2 M0	Loss of *MSH2* and *MSH6*, *KRAS* c.38G>A p.(Gly13Asp) detected in the transverse tumor	Unchecked
Combat CRC 009	Streck	Colorectal	330	Colon (hepatic flexure)	T3 N0 M0	MMR immunohistochemistry not performed	Unchecked
Combat CRC 010	Streck	Colorectal	235	Colon (ascending)	T3 N0 M0	Loss of *MLH1* and *PMS2*, *PIK3CA* c.3140A>G p.(His1047Arf)	Unchecked
Combat CRC 011	Streck	Colorectal	150	Colon (sigmoid)	Unavailable	*KRAS* c.183A>Tp.(Gln61His), *TP53* c.1024C>T p.(Arg342)	Neo-adjuvant chemotherapy (oxaliplatin and capecitabine)
Combat CRC 012**	Streck	Colorectal	346	Colon (sigmoid)	T3 N0 M0	*NRAS* codon 12 variant detected	Unchecked
Combat CRC 013	Streck	Colorectal	460	Caecum	T3 N2 M0	*KRAS* variant	Unchecked

Table S4: Clinical information for patients with gastrointestinal carcinoma used for whole genome sequencing study (*n* = 13).

APER, Abdomino Perineal Excision of Rectum; cm, centimeter; FLOT, Combination of chemotherapy drugs: docetaxel, oxaliplatin, 5-fluorouracil and leucovorin;
R-CHOP, Combination of chemotherapy: riituximab, cyclophosphamide, hydroxydaunorubicin hydrochloride (doxorubicin hydrochloride), vincristine (Oncovin) and prednisone;
MMR, mismatch repair

*Copy number variations were detected in the cfDNA and s-pDNA for this patient

** Sample used for targeted mutational analysis

Patient ID	Blood collection tube	Age (years)	Gestation (weeks + days)	Neonatal sex
AS/001	Streck	40	39 + 0	M
AS/002	Streck	32	39 + 3	F
AS/003	Streck	34	39 + 1	M
AS/004	Streck	34	40 + 4	F
AS/005	Streck	24	39 + 6	M
AS/006	Streck	39	40 + 4	F
AS/007	Streck	29	39 + 4	F
AS/008	Streck	32	39 + 2	M
AS/009	Streck	34	41 + 5	M
AS/010	Streck	32	35 + 4	M
AS/011	Streck	34	40 + 0	F
AS/012	Streck	33	35 + 1	F
AS/013	Streck	47	38 + 2	M
AS/014	Streck	40	39 + 0	M
AS/015	Streck	37	39 + 3	F
AS/016	Streck	40	39 + 0	M
AS/017	Streck	33	39 + 0	F
AS/018	Streck	29	41 + 3	F
AS/019	Streck	34	39 + 0	M
AS/020	Streck	34	39 + 0	M
PN/024	Streck	31	PD + 1	M
PN/025	Streck	36	PD + 2	M
PN/026	Streck	33	PD + 1	M
PN/027	Streck	31	PD + 1	F
PN/028	Streck	32	PD + 2	M
PN/029	Streck	40	PD + 1	M
PN/030	Streck	32	PD + 1	M
PN/031	Streck	34	PD + 1	M
PN/032	Streck	24	PD + 1	M
PN/033	Streck	31	PD + 2	M

Table S5: Clinical information for obstetric cohort (*n* = 30).

AS, antenatal sample; F, female; M, male; PD, post-delivery; PN, postnatal

Patient ID	Blood collection tube	Platelet count (x10^9/L)
ITP/001	Streck	3
ITP/002	Streck	490
ITP/003	Streck	18
ITP/004	Streck	31
ITP/005	Streck	157
ITP/007	Streck	35
ITP/008	Streck	34
ITP/014	Streck	80
ITP/015	Streck	17
ITP/016	Streck	21
ITP/017	Streck	42
ITP/018	Streck	231
ITP/020	Streck	12
ITP/021	Streck	76
ITP/022	Streck	10
ITP/023	Streck	2
ITP/024	Streck	18
ITP/025	Streck	27
ITP/026	Streck	256
ITP/027	Streck	52
ITP/028	Streck	375
ITP/029	Streck	465
ITP/030	Streck	335

Table S6: Clinical information for the immune thrombocytopenic purpura patients and controls cohort (*n* = 23).

ITP, immune thrombocytopenic purpura

Flow Cytometry					
Nucleic acid stain or antibody	**Clone**	**Conjugate**	**Dilution**	**Company**	**Catalog number**
CD42b	HIP1	FITC	1:20	BioLegend‡	303903
CD42	HIP1	PeCy7	1:20	BioLegend‡	303916
CD41	HIP8	PE-Cyanine7	1:30	BioLegend‡	303718
CD3	SK7	PE	1:20	BioLegend‡	344805
CD3	OKT3	BV421	1:20	BioLegend‡	317344
CD11b	ICRF44	APC	1:20	BioLegend‡	301309
CD33	WM53	APC	1:20	BioLegend‡	303407
CD19	HIB19	APC-Cyanine7	1:20	BioLegend‡	302218
CD235a	HIR2	BV650	1:20	BD Biosciences§	740583
CD235a	HIR2	FITC	1:20	Invitrogen#	11-9987-82
DAPI (4',6-Diamidino-2-Phenylindole, Dilactate)			1:100*	Invitrogen#	D3571
CD63	H5C6	PB	1:20	BioLegend‡	353012
CD62P	AK4	BV785	1:20	BioLegend‡	304941
SYTO 13 Green Fluorescent Nucleic Acid Stain			1:20	Invitrogen#	S7575
DRAQ5 Fluorescent Probe Solution			1:1200	BioLegend‡	424101
Microscopy					
Nucleic acid stain or antibody	**Clone**	**Conjugate**	**Dilution**	**Company**	**Catalog number**
SiR-DNA			1:500	Spirochromeˆ	SC007
NUCLEAR-ID Red DNA stain			1:2000	Enzo Life Sciences~	ENZ-2406
DRAQ5 Fluorescent Probe Solution			1:1000	BioLegend‡	424101
Hoechst 33342, Trihydrochloride Trihydrate			1:1000	Invitrogen#	H3570
Primary mouse anti-human CD63	MX-49.129.5	Unconjugated	1:50	Abcam†	ab193349

Table S7: Flow cytometry antibodies used for hematopoietic lineage panel, platelet activation panel, analysis of platelet DNA and RNA content and antibodies and nucleic acid stains used for microscopy.

Microscopy					
Nucleic acid stain or antibody	**Clone**	**Conjugate**	**Dilution**	**Company**	**Catalog number**
Primary mouse anti-human LAMP2	H4B4	Unconjugated	1:100	Abcam†	ab25631
Primary mouse anti-human CD62P	AK-6	Unconjugated	1:55	Abcam†	ab6632
Primary rabbit anti-human CD81	EPR21916	Unconjugated	1:100	Abcam†	ab219209
Primary rabbit IgG anti-human TOM20 (D8T4N)	Recombinant (D8T4N)	Unconjugated	1:200	Cell signalling technology¦	42406S
Primary anti-β-Tubulin mouse monoclonal	TUB 2.1	Unconjugated	1:130	Sigma Aldrich°	T5201
Primary anti-mouse p53	1C12	Unconjugated	1:2000	Cell signalling technology¦	2524
Secondary goat anti-mouse IgG H&L		AF568	1:500 or 1:1000	Abcam†	ab175473
Secondary goat anti-rabbit IgG H&L		AF488	1:500	Cell signalling technology¦	4412
Secondary donkey anti-mouse IgG H&L		AF405	1:1000	Abcam†	ab175658
Secondary horse anti-mouse IgG		HRP-linked	1:100	Cell signalling technology¦	7076

Table S7: Flow cytometry antibodies used for hematopoietic lineage panel, platelet activation panel, analysis of platelet DNA and RNA content and antibodies and nucleic acid stains used for microscopy (continued).

*Viability stain, previously diluted 1:100 from 5 mg/ml stock solution

§Becton, Dickinson and Company, Franklin Lakes, US-NJ

‡BioLegend, San Diego, US-CA

#Invitrogen (Thermo Fisher Scientific Inc.,) Waltham, US-MA

ˆSpirochrome, Switzerland

~Enzo Life Sciences (UK) LTD, UK

†Abcam, Cambridge, UK

¦Cell Signalling Technology, Inc., Danvers, US-MA

°Sigma Aldrich, St. Louis, US-MO

SUPPLEMENTARY MOVIE LEGENDS

Movie S1: 3D render of maternal platelet labeled with β-tubulin (blue), with positive signal for a Y-chromosome fluorescent *in situ* hybridization (FISH) probe (orange).

Movie S2: Live cell imaging video showing uptake of fluorescently labeled DNA (magenta) from a COLO205 cell by a platelet from a healthy donor *in vitro*.

Movie S3: Live cell imaging video showing multiple platelets (stained with CD42 488 [blue]) showing signal for fluorescently labeled DNA (magenta) derived from COLO205 cells *in vitro*.

Movie S4: 3D render and rotation video of a platelet (stained with CD42 488 [blue]) with adherent extracellular vesicle (EV) (succinimidyl ester [SE], red) containing DNA (DAPI, yellow).

Movie S5: 3D render and rotation video of a platelet (stained with CD42 488 [blue]) with internal extracellular vesicle (EV) (succinimidyl ester [SE], red) containing DNA (DAPI, yellow).

Movie S6: Live cell imaging video of healthy donor platelets (CD42 AF488, cyan) incubated with H2B-mCh HEL cells genetically engineered to express mCherry-tagged histones (magenta). White arrow shows platelet sequestration of tumor cell-derived histones (magenta) and DNA (DAPI, yellow). Scale bar represents 5 μm, imaged using a Zeiss Spinning Disk Confocal with a 63X oil immersion objective.